Rate Constants for the Thermal Decomposition of Ethanol and Its Bimolecular Reactions with OH and D: Reflected Shock Tube and Theoretical Studies

R. Sivaramakrishnan, M.-C. Su,† J. V. Michael,* S. J. Klippenstein,* L. B. Harding, and B. Ruscic

Chemical Sciences and Engineering Division, Argonne National Laboratory, Argonne, Illinois 60439

Received: May 24, 2010; Revised Manuscript Received: July 15, 2010

The thermal decomposition of ethanol and its reactions with OH and D have been studied with both shock tube experiments and ab initio transition state theory-based master equation calculations. Dissociation rate constants for ethanol have been measured at high *T* in reflected shock waves using OH optical absorption and high-sensitivity H-atom ARAS detection. The three dissociation processes that are dominant at high *T* are

$$C_2H_5OH \rightarrow C_2H_4 + H_2O \quad (A)$$

$$\rightarrow CH_3 + CH_2OH \quad (B)$$

$$\rightarrow C_2H_5 + OH \quad (C)$$

The rate coefficient for reaction C was measured directly with high sensitivity at 308 nm using a multipass optical White cell. Meanwhile, H-atom ARAS measurements yield the overall rate coefficient and that for the sum of reactions B and C, since H-atoms are instantaneously formed from the decompositions of CH_2OH and C_2H_5 into $CH_2O + H$ and $C_2H_4 + H$, respectively. By difference, rate constants for reaction 1 could be obtained. One potential complication is the scavenging of OH by unreacted ethanol in the OH experiments, and therefore, rate constants for

$$OH + C_2H_5OH \rightarrow \text{products} \quad (D)$$

were measured using *tert*-butyl hydroperoxide (*t*BH) as the thermal source for OH. The present experiments can be represented by the Arrhenius expression

$$k = (2.5 \pm 0.43) \times 10^{-11} \exp(-911 \pm 191 \text{ K/T}) \text{ cm}^3 \text{ molecule}^{-1} \text{ s}^{-1}$$

over the *T* range 857−1297 K. For completeness, we have also measured the rate coefficient for the reaction of D atoms with ethanol

$$D + C_2H_5OH \rightarrow \text{products} \quad (E)$$

whose H analogue is another key reaction in the combustion of ethanol. Over the *T* range 1054−1359 K, the rate constants from the present experiments can be represented by the Arrhenius expression,

$$k = (3.98 \pm 0.76) \times 10^{-10} \exp(-4494 \pm 235 \text{ K/T}) \text{ cm}^3 \text{ molecule}^{-1} \text{ s}^{-1}$$

The high-pressure rate coefficients for reactions B and C were studied with variable reaction coordinate transition state theory employing directly determined CASPT2/cc-pvdz interaction energies. Reactions A, D, and E were studied with conventional transition state theory employing QCISD(T)/CBS energies. For the

10.1021/jp104759d
Published on Web 08/18/2010

saddle point in reaction A, additional high-level corrections are evaluated. The predicted reaction exo- and endothermicities are in good agreement with the current Active Thermochemical Tables values. The transition state theory predictions for the microcanonical rate coefficients in ethanol decomposition are incorporated in master equation calculations to yield predictions for the temperature and pressure dependences of reactions A−C. With modest adjustments (<1 kcal/mol) to a few key barrier heights, the present experimental and adjusted theoretical results yield a consistent description of both the decomposition (1−3) and abstraction kinetics (4 and 5). The present results are compared with earlier experimental and theoretical work.

Introduction

Ethanol, C_2H_5OH, is an important alternative renewable combustion fuel and is now commonly used as an additive, extender, and oxygenate for transportation energy needs. It can and already has been used as a neat fuel. It also serves as a simple prototype for more complex alcohols, such as butanol, that are being considered as next generation biofuels. Because of this interest, many experimental studies of both its pyrolysis and oxidation have been carried out using a variety of techniques, and theoretical studies have been applied to understand these results. These early studies have been thoroughly reviewed by Marinov,[1] Park et al.,[2] Li et al.,[3] and Tsang.[4]

Using G2M theory, Park et al.[2] have suggested 11 endothermic decomposition pathways,

$$C_2H_5OH \rightarrow C_2H_4 + H_2O \quad (1)$$

$$\rightarrow CH_3 + CH_2OH \quad (2)$$

$$\rightarrow C_2H_5 + OH \quad (3)$$

$$\rightarrow CH_3CHO + H_2 \quad (4)$$

$$\rightarrow C_2H_3OH + H_2 \quad (5)$$

$$\rightarrow CH_4 + H_2CO \quad (6)$$

$$\rightarrow CH_4 + CHOH \quad (7)$$

$$\rightarrow CH_3CH + H_2O \quad (8)$$

$$\rightarrow C_2H_5O + H \quad (9)$$

$$\rightarrow CH_3CHOH + H \quad (10)$$

$$\rightarrow C_2H_4OH + H \quad (11)$$

Using multichannel unimolecular rate theory, they narrow these possibilities down to four processes, reactions 1−3 and reaction 8. On the basis of additional energy estimates,[3,4] most other authors conclude that only the first three reactions are important at high-T.

Surprisingly, there are no direct kinetics studies of the title reactions using shock waves at the high temperatures encountered in combustion. Single-pulse shock wave experiments have been performed on the total rate of decomposition,[5] and measurements of $[H_2O]_t$ and $[CO]_t$ by FTIR, when simulated with a 180 reaction step mechanism, gave decomposition rate constants.[6] Here, we make the first measurements of the OH radical formation rates due to reaction 3 using OH radical optical absorption at 308 nm. We then study H-atom formation rates using H-atom atomic resonance absorption spectrometry (ARAS), and with the known rate constants for reaction 3 from the OH experiments, rate constants for reaction 1 and 2 are obtained.

We have also performed a high-level theoretical analysis of the decomposition kinetics. This analysis builds on the earlier efforts of Lin and co-workers[2] and of Dryer and co-workers[3] by incorporating higher-level estimates for the transition state energies and employing the more accurate variable-reaction-coordinate transition-state-theory (VRC-TST) approach[7,8] in the treatment of the barrierless radical−radical channels. Furthermore, the present experimental results allow for a more definitive parametrization of the falloff effects through fits to the results of master equation calculations.

In this work, we have also studied experimentally the abstraction reaction,

$$OH + C_2H_5OH \rightarrow \text{products} \quad (12)$$

because it is an important OH radical terminating step in the lower-T range of the present experiments. Furthermore, for completeness, we have also measured abstraction rate constants for

$$D + C_2H_5OH \rightarrow \text{products} \quad (13)$$

The H analog of this reaction is another key reaction in the pyrolysis and oxidation of ethanol.

We also make transition state theory predictions for the rate coefficients in these two abstraction reactions, 12 and 13. This theoretical analysis allows for meaningful extrapolations of the experimental data to higher and lower temperatures than accessible experimentally. It also provides a measure of the product branching in both reactions and allows us to examine the isotope dependence for reaction 13. These predictions again build on the earlier work of Lin and co-workers[9,10] with the incorporation of higher-level estimates of the interaction energies and more complete considerations of the torsional motions.

Experiment

The present experiments were performed with the reflected shock tube technique using both OH radical electronic absorption and H-atom ARAS detection. The methods and the apparatus currently being used have been previously described,[11,12] and only a brief description of the experiment will be presented here.

For the OH-radical experiments, the shock tube was fabricated from 304 stainless steel in three sections; however, for the H-atom experiments, the shock tube was constructed entirely from a 7-m (10.2 cm o.d.) 304 stainless steel tube. In both configurations, a 10.2 cm-o.d. cylindrical section was separated from the He driver chamber by a 4 mil unscored 1100-H18 aluminum diaphragm, but for the OH apparatus, a 0.25 m transition section then connected the first and third sections. The third section was of rounded corner (radius, 1.71 cm) square design and was fabricated from flat stock (3 mm) with a mirror

* To whom correspondence should be addressed: E-mail: (J.V.M.) jmichael@anl.gov, (S.J.K.) sjk@anl.gov.
† Special Term Appointment, Argonne. Permanent address: Department of Chemistry, Sonoma State University,1801 E. Cotati Ave., Rohnert Park, CA 94928.

finish. In both configurations, the tubes were routinely pumped between experiments to less than 10^{-8} Torr by an Edwards Vacuum Products model CR100P packaged pumping system. Shock wave velocities were measured with eight equally spaced pressure transducers (PCB Piezotronics, Inc., model 113A21) mounted along the downstream part of the test section and recorded with a 4094C Nicolet digital oscilloscope. Temperature and density in the reflected shock wave regime were calculated from this velocity. This procedure has been given previously, and corrections for boundary layer perturbations have been applied.[13−15] The oscilloscopes were triggered by a signal pulse derived from the last velocity gauge mounted on the end plate. In both cases, the photometer systems were radially located at 6 cm from the end plate.

For the OH-radical experiments, a White cell, as described previously,[16−18] was used to increase the absorption path length. The White cell was constructed from two flat fused-silica windows (3.81 cm), mounted on the tube across from one another, with broadband antireflection (BB AR) coating for UV light. The distance between windows was 8.745 cm. The optical configuration consisted of an OH resonance lamp,[16,17] multipass reflectors, an interference filter at 308 nm, and a photomultiplier tube (1P28), all mounted external to the shock tube. Signals were recorded by a LeCroy model LC334A oscilloscope.

At the entrance to the multipass cell, OH resonance radiation was collimated with a set of lenses and was focused onto the reflector on the opposite side of the shock tube through the two AR-coated windows that were flush-mounted to the inside of the shock tube. The reflectors and windows were obtained from the CVI Laser Corporation. These reflectors were attached to adjustable mounts, and the center points of windows and mirrors were all in a coaxial position. With this new configuration, multiple passes were used, thereby amplifying the measured absorbances by a factor of ∼4.5 over that used in the previous work.[17,18] This increase in sensitivity for OH-radical detection allows for the detection of lower [OH] and therefore decreases the importance of secondary reaction perturbations.

For H(D)-atom detection, the lenses were crystalline MgF_2, and the resonance lamp beam intensity (filtered through 6 cm of dry air (21% O_2) to isolate the Lyman-α_H or Lyman-α_D wavelengths at 121.6 nm), was measured by an EMR G14 solar blind photomultiplier tube, as described previously,[19−21] and recorded with a LeCroy model LC334A oscilloscope. To measure the fraction of non-Lyman-α_H present in the resonance absorption emission lamp, an H_2 discharge flow system was used to create large [H] between the lamp and shock tube window,[19] thereby removing all of the resonance lamp emission. The H-atom experiments were then performed with the discharge system turned off.

The D-atom experiments required metering very small amounts of D_2 into the resonance lamp such that the lamp intensity was similar to that for H-atoms. This ensures that the D-atom lamp will then be effectively unreversed; that is, a Gaussian distribution.[21] In this case, D-atoms in the presence of H-atoms can be directly detected by carrying out the experiment with the H_2 discharge flow system turned on (i.e., removing Lyman-α_H) during the D-atom experiment.

Gases. High-purity He (99.995%), used as the driver gas, was from AGA Gases. Scientific grade Kr (99.999%), the diluent gas in reactant mixtures, was from Spectra Gases, Inc. The ∼10 ppm impurities (N_2, 2 ppm; O_2, 0.5 ppm; Ar, 2 ppm; CO_2, 0.5 ppm; H_2, 0.5 ppm; CH_4, 0.5 ppm; H_2O, 0.5 ppm; Xe, 5 ppm; and CF_4, 0.5 ppm) are all either inert or in sufficiently low concentration that they do not perturb either OH-radical or H-atom profiles. For OH detection, the microwave-driven OH lamp operated at 70 W and ∼25 Torr pressure. Distilled water, evaporated at 1 atm into ultrahigh-purity grade Ar (99.999%) from AGA Gases, was used in the resonance lamp. For H atoms, the microwave-driven resonance lamp operated at 35 W and 1.9 Torr of ultrahigh-purity He (99.999%), which contains a trace of hydrogenous impurities that are sufficient to give measurable Lyman-α radiation.[21] For the D + C_2H_5OH experiments, C_2D_5I was the source of D-atoms and was supplied by Aldrich Chemical Inc. (reagent grade, ≥99.5%). Ethanol (>99.5% C_2H_5OH) was obtained from Pharmco-Aaper Inc. The principal impurities were methanol, acetaldehyde, and benzene, amounting to <0.5%. These compounds were further purified by bulb-to-bulb distillation, retaining only middle thirds for mixture preparation. T-HYDRO *tert*-butyl hydroperoxide (*t*BH, ∼70% *t*BH by weight water solution; i.e., ∼32 mol % *t*BH and 68 mol % H_2O) was obtained from the Aldrich Chemical Co. Inc. and was used as the OH radical source for the OH + C_2H_5OH reaction studies as described previously.[22] The gas mixtures were accurately prepared from pressure measurements using a Baratron capacitance manometer and were stored in an ultrahigh-purity, all glass vacuum line.

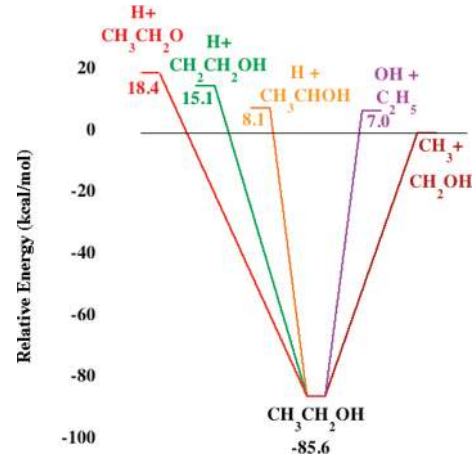

Figure 1. Schematic plot of the potential energy surface for the simple bond fissions in ethanol.

Theory

C_2H_5OH Decomposition. Zero-point corrected schematic potential energy surfaces for the decomposition of ethanol are shown in Figure 1 for the simple bond fissions to produce two radicals and in Figure 2 for the molecular decompositions with tight transition states. The energies for these plots come from QCISD(T)/CBS calculations[23] in which the basis set extrapolation is based on calculations with the cc-pVTZ and cc-pVQZ basis sets of Dunning.[24,25] The underlying geometries and rovibrational properties for the transition state theory (TST) analyses are largely obtained with B3LYP/6-311++G** density functional theory.[26] However, for channel 8, there are significant differences in spin-restricted and unrestricted B3LYP/6-311++G** geometries. Thus, for this channel, the rovibrational properties are instead obtained at the CASPT2/aug-cc-pVTZ level,[27,28] where the CO and active CH bonds are included in the 4 electron 4 orbital (4e, 4o) active space of the CAS part of the calculation. Notably, the T1 diagnostics[29] for these channels are all 0.027 or lower, and so one does not expect significant errors in the QCISD(T) analysis arising from multireference effects on the wave functions. For the C_2H_5 + OH channel, we include a spin−orbit correction for OH of −0.11 kcal/mol.

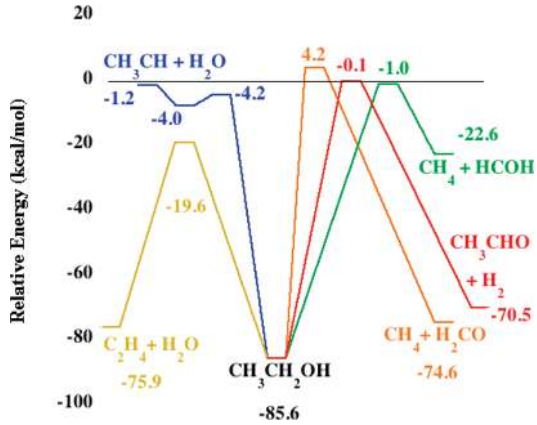

Figure 2. Schematic plot of the potential energy surface for the molecular fissions in ethanol.

This potential energy surface was previously studied in considerable detail by Park et al.[2] at the G2M level.[30] More limited calculations for the primary channels were reported by Li et al.[3] at the G3B3[31] level and are supplemented with additional calculations here. The present QCISD(T)/CBS predictions for the zero-point corrected stationary point energies are compared with the corresponding G2M, G3B3, and CBS-APNO[32] values in Table 1. For the stable species, Active Thermochemical Tables (ATcT)[33,34] values, developed in concert with the current study, are also reported in Table 1. Notably, the QCISD(T)/CBS predictions for the stable species, with an rms error of only 0.3 kcal/mol, are in markedly better agreement with the ATcT values than the G2M values, for which the rms error is 2.6 kcal/mol. The present QCISD(T)/CBS predictions also provide a modest improvement in accuracy over the G3B3 and CBS-APNO energies. This improvement is largely due to the removal of various additivity approximations in the G3B3 and CBS-APNO methods. Similar, if not greater, improvements are expected for the predicted barrier heights, where the additivity approximations may be less reliable and the structural determinations are more sensitive to the method used for the geometry optimization.

The $CH_3 + CH_2OH$ channel (2), which is the lowest-energy simple bond fission channel, is taken as the zero of energy for the plots in Figures 1 and 2. The three CH fission channels (9, 10, and 11) are higher in energy than the CC (2) and CO (3) fission channels. Furthermore, fissions to produce atoms generally have a lower entropy than those to produce two polyatomics. Thus, channels 9, 10, and 11 are not expected to contribute significantly to the kinetics and are not considered further here.

The saddlepoints for the molecular fissions to produce $H_2 + CH_3CHO$ (4), $CH_4 + H_2CO$ (6), and $CH_4 + CHOH$ (7), respectively, are all close to (within −1.0 kcal/mol) or higher than the $CH_3 + CH_2OH$ channel (2). Furthermore, the tight transition states for these channels have much lower entropy than that for the barrierless CC fission channel (2). Thus, these tight transition states are also not expected to contribute significantly to the kinetics and were not considered further here.

However, other roaming radical pathways[35] should exist for these three channels (4, 6, and 7). For example, $CH_4 + H_2CO$ (6) may be produced by a near CC fission followed by a reorientation of the incipient CH_3 radical to an orientation that allows for the direct abstraction of an H atom from the OH portion of the incipient CH_2OH radical. Similar pathways should exist for channels 7 and 4. Our recent combined theory and experiment study on the decomposition of acetaldehyde[36,37] suggests, together with other work in progress for related reactions such as the decomposition of propane, that the contribution from such roaming radical pathways is typically ∼10−20% that for the corresponding simple bond fission. For the conditions of interest here, these simple bond fissions, although significant, are never dominant. Thus, for simplicity, we have chosen to neglect such roaming radical pathways in the present analysis. For similar reasons, the corresponding roaming radical pathways to channels 1 and 5 are also neglected here.

The pressure-dependent kinetics is studied with ab initio transition state theory-based master equation simulations. The master equation simulations were performed as described in refs 38 and 39. They employ Lennard-Jones collision rates and an exponential down energy transfer model. The calculations are analogous to those described in our recent study of the CH_3OH decomposition.[40] As discussed above and illustrated in Figure 3, this analysis considers only channels 1−3 and 8. These theoretical calculations proceed beyond those of refs 1−4 in

TABLE 1: Stationary Point Energies for the Decomposition of C_2H_5OH[a]

stationary point	QCISD(T)/CBS[b]	G2M[c]	G3B3[b,d]	CBS-APNO[b]	ATcT[b]
$CH_3 + CH_2OH$	85.6	87.5	84.6	85.6	85.33 ± 0.11
$CH_3CH_2 + OH$	92.6[e]	94.8	*91.5*[e]	92.6[e]	92.05 ± 0.10
$CH_3CHOH + H$	93.7		*93.4*	93.6	93.46 ± 0.14[f]
$CH_2CH_2OH + H$	100.7		*100.3*	101.1	100.46 ± 0.14[g]
$CH_3CH_2O + H$	104		*103.5*	103.8	103.93 ± 0.11[h]
$C_2H_4 + H_2O$	9.7	6.5	9.4	10.4	9.33 ± 0.06
$C_2H_5OH \rightarrow C_2H_4 + H_2O$	66.0	66.6	66.6		
$^1CH_3CH + H_2O$	84.4	80.3	*84.3*	85.3	84.26 ± 0.27
$^1CH_3CH\cdots H_2O$[i]	81.4	81.3			
$C_2H_5OH \rightarrow {}^1CH_3CH\cdots H_2O$[i]	81.6	82.9			
$CH_4 + CHOH$	63.0	65.8	*62.4*	63.3	62.68 ± 0.12[j]
$C_2H_5OH \rightarrow CH_4 + CHOH$	84.6	84.3			
$CH_3CHO + H_2$	15.1	14.7	*14.1*	14.7	14.79 ± 0.08
$C_2H_5OH \rightarrow CH_3CHO + H_2$	85.5	86.0			
$CH_4 + H_2CO$	11	9.1	*10.1*	10.7	10.75 ± 0.06
$C_2H_5OH \rightarrow CH_4 + H_2CO$	89.8	99.7			
rms Error[k]	0.30	2.62	0.45	0.56	

[a] Values are in kcal/mol relative to the most stable (staggered) conformer of C_2H_5OH and include zero-point corrections. [b] Present work. ATcT values are from C(A)TN version 1.110. [c] From ref 2. [d] From ref 3 as available. Italic values are from the present work. In addition, the value of 84.3 kcal/mol for $CH_3 + CH_2OH$ in ref 2 is corrected to 84.6 kcal/mol here. [e] Corrected for spin−orbit (i.e., rotational zero-point energy) of OH by −0.11 kcal/mol. [f] *gauche-anti*-CH_3CHOH. [g] *gauche-syn*-CH_2CH_2OH. [h] X $^2A''$ CH_3CH_2O. [i] van der Waals complex between $^1CH_3CH$ and H_2O. [j] *trans*-CHOH. [k] Root-mean-squared error relative to ATcT values as available.

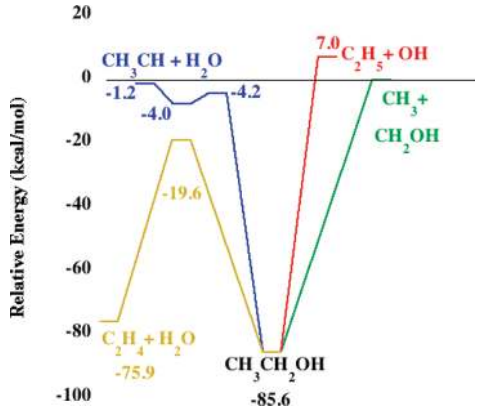

Figure 3. Schematic plot of the potential energy surface for the channels employed in the master equation treatment of the decomposition of ethanol.

employing higher level ab initio estimates and more sophisticated transition state theory treatments within the detailed master equation simulations.

The CH_3CH product in channel 8 is expected to rapidly isomerize to ethylene, which makes channel 8 essentially equivalent to channel 1. Thus, in the presentation of the results, the rate coefficients for channels 1 and 8 are summed together. The microcanonical and J-resolved rate coefficients for channel 1 and 8 are evaluated with conventional transition state theory. An asymmetric Eckart tunneling correction is included for channel 1, since it has the lowest threshold and because the large value for the imaginary frequency (2100 cm^{-1}) results in a significant correction up to moderately high temperature. The state densities for the various species include hindered rotor partition functions for the torsional modes as appropriate.

The saddlepoint for channel 8 is "submerged" with respect to the asymptotic energy for this channel. Correspondingly, there are two transition states for this channel: one loose outer transition state at large separations of importance at low energy and a traditional tight inner transition state in the neighborhood of the saddle point. Due to the much lower energy for channel 1, channel 8 can be of significance only at high energies, but at high energies, the inner transition state for channel 8 provides its dominant bottleneck. Thus, we consider only the inner transition state in evaluating the reactive flux for channel 8.

Channels 2 and 3 are studied with direct variable reaction coordinate transition state theory.[41] For the CC bond fission (channel 2) the orientation dependent energies are obtained from CASPT2(2e,2o)/cc-pVDZ calculations. The active orbitals consist of the methyl and hydroxymethyl radical orbitals. A one-dimensional correction based on higher-level calculations for related CC bond fissions is incorporated. For the CO bond fission (channel 3), the orientation-dependent energies are obtained from state-averaged CASPT2(4e,3o)/cc-pVDZ calculations. The active orbitals consist of the ethyl radical orbital and the π orbitals of OH, and the state averaging is over the two states correlating with the orbital degenerate states of OH. Test calculations with the aug-cc-pVDZ basis suggest little basis set dependence. Both front and back side attacks were considered for each of these channels. The final results incorporate a dynamical correction factor of 0.85.[41]

The initial implementation of this ab initio TST based master equation analysis yields total rate coefficients that are significantly lower than the experimental measurements. These rate coefficients are about a factor of 3 lower than the measurements of Li et al.[3] near 1050 K. Reducing the barrier to formation of $C_2H_4 + H_2O$ by 2.2 kcal/mol would reproduce these low temperature rate coefficients as well as those of Herzler et al.,[5] but such an error in the barrier height is at the limit of what might be expected for the present level of theory. For this reason, we have further explored this transition state with additional higher-level calculations. For reference purposes, we have also explored C_2H_5OH and the $CH_2OH + CH_3$ channel with the same methods.

This higher-level analysis starts with a reevaluation of the rovibrational properties at the QCISD(T)/cc-pVTZ level of theory. At these geometries, we have (i) obtained an improved estimate of the CBS limit from calculations with the cc-pVQZ and cc-pV5Z bases, (ii) obtained a correction for higher-order excitations with calculations at the CCSDT(Q)/cc-pVDZ level (employing the MRCC module of Kállay[42,43]), and (iii) obtained a correction for core−valence correlation from CBS limit estimates employing the cc-pCVTZ and cc-pCVQZ bases.[44] For the saddle point relative to C_2H_5OH, these three corrections are 0.11, −0.53, and 0.21 kcal/mol, respectively. Meanwhile, for $CH_3 + CH_2OH$ relative to C_2H_5OH, these corrections are −0.23, −0.08, and −0.13 kcal/mol, respectively. The net result is that, relative to C_2H_5OH, the saddle point energy for the dominant channel is predicted to be lower by 0.22 kcal/mol, whereas the $CH_3 + CH_2OH$ products are predicted to be lower by 0.48 kcal/mol. The latter correction changes the $CH_3 + CH_2OH$ energy from being 0.25 kcal/mol higher than the ATcT value to being 0.23 kcal/mol lower than it.

The final analysis employs these QCISD(T)/cc-pVTZ frequencies, since they are expected to be more reliable than the B3LYP/6-311++G(d,p) values. In reality, there is little distinction between the two. The final analysis also uses these higher level energy estimates as a primary reference. For the $C_2H_5 +$ OH channel, we employ the Active Thermochemical Tables value for the energy relative to C_2H_5OH. The remaining uncertainty in the saddle point energy is expected to be ∼1 kcal/mol.

OH + CH_3CH_2OH and D + CH_3CH_2OH. The rovibrational properties of the reactants and the saddlepoints for the direct abstractions of the three chemically distinct H atoms in ethanol by OH and H/D were studied at the CASPT2(3e, 3o) level, employing the aug-cc-pVTZ basis for the abstractions by H/D and the primary channel in the abstraction by OH. For the secondary channels in the abstraction by OH, the smaller aug-cc-pVDZ basis was instead employed. The active space for these CASPT2 calculations consisted of the radical orbital of OH or H and the σ, σ^* orbital pair for the H being abstracted. Explicit optimizations were performed for the various torsional modes in the reactants and in the abstraction transition states. The rovibrational properties for the reactant and product van der Waals complexes in the C_2H_5OH + OH reaction were obtained at the CASPT2/aug-cc-pVDZ level. For the reactant van der Waals complex, the CAS calculation involved a state-averaged (3e, 2o) active space consisting of the two π orbitals of the OH radical. For the product van der Waals complexes the (1e, 1o) active space included only the radical orbital of the product. The rovibrational properties of the products were determined with the B3LYP/6-311++G(d,p) density functional method.

Higher-level energies for these stationary points were obtained from spin-restricted QCISD(T)/CBS calculations at these optimized geometries and are reported in Tables 2 and 3 for the abstractions by OH and H, respectively. Related CCSD(T)/6-311+G(3df,2p)//MP2/6-311+G(3df,2p) energies from Xu and Lin,[9] and CCSD(T)/6-311G(d,p)//BHandHLYP/6-311G energies from Galano et al.[45] are also provided in Table 2, while G2M(RCC2) calculations from Park et al.[10] are also reported

TABLE 2: Stationary Point Energies for the Reaction of C_2H_5OH with OH[a]

saddle point	QCISD(T)/CBS[b]	CCSD(T)/6-311+G(3df,2p)[c]	CCSD(T)/6-311G(d,p)[d]
$C_2H_5OH\cdots OH$	−4.3	−5.1	
$C_2H_5OH + OH \rightarrow CH_3CHOH + H_2O$	−0.1	−0.6	0.4
$CH_3CHOH\cdots H_2O$	−28.9	−26.3	
$CH_3CHOH + H_2O$	−24.2	−22.9	
$C_2H_5OH + OH \rightarrow CH_2CH_2OH + H_2O$	1.3	1.8	2.6
$CH_2CH_2OH\cdots H_2O$	−20.6	−19.6	
$CH_2CH_2OH + H_2O$	−17.2	−15.5	
$C_2H_5OH + OH \rightarrow CH_3CH_2O + H_2O$	3.7	3.4	3.0
$CH_3CH_2O\cdots H_2O$	−16.4	−17.3	
$CH_3CH_2O + H_2O$	−13.9	−13.3	

[a] Values are in kcal/mol relative to C_2H_5OH + OH and include zero-point corrections. [b] Present QCISD(T)/CBS calculations including SO correction. The saddlepoint and van der Waals complex energies are obtained at CASPT2(3,3) geometries, and the products are obtained at B3LYP/6-311++G(d,p) geometries. [c] CCSD(T)/6-311+G(3df,2p)//MP2/6-311+G(3df,2p) from Xu and Lin.[9] [d] CCSD(T)/6-311G(d,p)//MP2/6-311G(d,p) from Galano et al.[45]

TABLE 3: Stationary Point Energies for the Reaction of C_2H_5OH with H/D[a]

saddle point	QCISD(T)/CBS[b]	G2M(RCC2)[c]
$C_2H_5OH + H \rightarrow CH_3CHOH + H_2$	6.0 (5.4)	7.2
$CH_3CHOH + H_2$	−9.6	−7.7
$C_2H_5OH + H \rightarrow CH_2CH_2OH + H_2$	10.4 (9.6)	13.3
$CH_2CH_2OH + H_2$	−2.6	−1.2
$C_2H_5OH + H \rightarrow CH_3CH_2O + H_2$	13.4 (12.3)	15.0
$CH_3CH_2O + H_2$	0.6	2.2

[a] Values are in kcal/mol relative to C_2H_5OH + H/D and include zero-point corrections. [b] Present QCISD(T)/CBS calculations. Saddlepoint energies were obtained at CASPT2(3,3)/aug-cc-pvtz geometries, while product energies were obtained at B3LYP/6-311++G(d,p) geometries. Primary entries are for H; values in parentheses are for D. [c] From Park et al.[10]

in Table 3. The present CASPT2/aug-cc-pVTZ geometries are expected to be more accurate than the MP2 and BHandHLYP geometries of the previous studies. More importantly, the present extrapolation to the basis set limit should provide considerably more accurate energy predictions than in these prior works, particularly that of ref 45, where only the relatively small 6-311G(d,p) basis is considered. The present predictions for the saddle point energies differ from the previous predictions by amounts ranging from 0.3 to 2.9 kcal/mol. Such differences have important kinetic effects.

For the C_2H_5OH + OH reaction, Galano et al.[45] predict an H-bonding configuration for the saddlepoint to produce $CH_2CH_2OH + H_2O$, whereas Xu and Lin[9] predict a more open non-H-bonded geometry. Our calculations find that the H-bonded saddlepoint lies 1.4 kcal/mol higher in energy than the geometry of Xu and Lin[9] and also has significantly less entropy. Thus, it is kinetically irrelevant.

The T1 diagnostics for the QCISD(T) calculations were 0.028 or lower, which implies negligible multireference effects, for all but the transition state for the abstraction by OH to form $CH_3CH_2O + H_2O$, where it was 0.047. The latter channel has a relatively high endothermicity and barrier and so is not expected to be a major channel. Thus, the moderately increased uncertainties for this channel are of little concern.

The partition functions for the torsional motions (two modes for C_2H_5OH and two or three modes as appropriate for the saddlepoints) were evaluated with Pitzer−Gwinn-like approximations for assumed separable 1-dimensional hindered rotors as in prior studies. Tunneling corrections are small (<20%) for the temperatures of primary interest here, that is, at 1000 K and higher. Nevertheless, for completeness and for the purposes of comparison with the low temperature experiments for the reaction with OH, we include asymmetric Eckart tunneling corrections in the kinetic analysis. For the OH reaction, the asymptote energies are set to the energies of the van der Waals pre- and postreactive complexes. For the reaction with H, these van der Waals complexes have only small binding energies, and for simplicity, we instead employ the energies of the bimolecular products for the tunneling asymptotes.

For the abstractions by OH, we incorporate a spin−orbit lowering of 0.11 kcal/mol for the ground state of the reactants and also include a correction to the reactant partition function related to the nonseparability of the electronic and rotational motions. These corrections presume that the spin−orbit splitting and rotational-electronic coupling has already become negligible at the transition state. They are of little significance at high temperature, but do have some bearing on the comparison with room temperature experiments for the C_2H_5OH + OH reaction.

For the $CH_3CHOH + H_2O$ channel in the reaction with OH, the calculated barrier lies just below the reactants. Thus, we also consider a loose phase space theory transition state for the van der Waals complex formation with an assumed rate constant of 4×10^{-10} cm^3 molecule^{-1} s^{-1}. Incorporating this outer transition state in a two transition-state minimum flux model reduces the rate by ∼10% at the lowest temperature (200 K) considered here. The smallness of this correction implies that a more accurate treatment of the outer transition state is not required.

Results

OH + CH_3CH_2OH. As has been pointed out in previous absolute rate constant studies,[46−58] there are three abstractable H-atoms in ethanol,

$$OH + CH_3CH_2OH \rightarrow CH_3CHOH + H_2O \quad (12a)$$

$$\rightarrow CH_2CH_2OH + H_2O \quad (12b)$$

$$\rightarrow CH_3CH_2O + H_2O \quad (12c)$$

yielding distinct radical products that subsequently react in entirely different ways. In most of these studies, the total rate constants have been determined; however, branching ratios between these processes have been measured in at least two of these reports.[48,51] There is a consensus that 12a should be the predominant abstraction reaction at all temperatures. Theoretical studies of Xu and Lin[9] on this reaction corroborate this conclusion giving a branching ratio for 12a at ∼200 K of 0.98. The theoretically predicted branching ratio decreases monotoni-

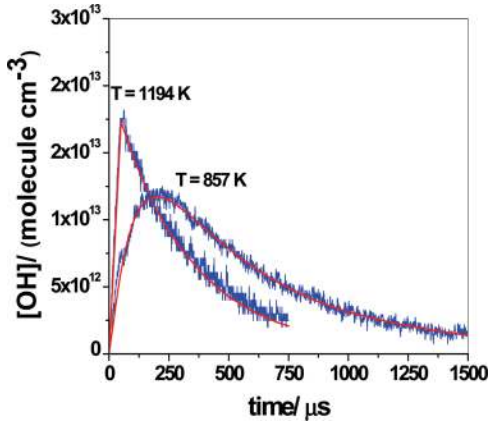

Figure 4. Two [OH] profiles at 1194 and 857 K, respectively. The solid lines are fits over the entire time range using the reaction mechanism of Table 4 with variations in k_{12}. The conditions for the experiment at $T_5 = 1194$ K are $P_1 = 15.92$ Torr, $M_s = 2.145$, $\rho_5 = 2.583 \times 10^{18}$ molecules cm^{-3}, $[t\text{BH}]_0 = 2.03 \times 10^{13}$ molecules cm^{-3}, $[H_2O]_0 = 4.52 \times 10^{13}$ molecules cm^{-3}, and $[C_2H_5OH]_0 = 2.42 \times 10^{14}$ molecules cm^{-3}. The conditions for the experiment at $T_5 = 857$ K are $P_1 = 30.98$ Torr, $M_s = 1.790$, $\rho_5 = 3.838 \times 10^{18}$ molecules cm^{-3}, $[t\text{BH}]_0 = 1.74 \times 10^{13}$ molecules cm^{-3}, $[H_2O]_0 = 3.61 \times 10^{13}$ molecules cm^{-3}, and $[C_2H_5OH]_0 = 1.87 \times 10^{14}$ molecules cm^{-3}.

cally to 0.80 ± 0.02 over the present experimental T range. Hence, at low T, the overall rate constants refer essentially to 12a, with 12b and 12c increasing in importance as temperature increases. The work of Hess and Tully[51] clearly shows at 700 Torr He between ~500 and 650 K that the radical product of 12b dissociates to C_2H_4 + OH. In this range, the profiles are biexponential becoming strictly first-order again above 650 K. Under the present conditions, reaction 12b followed by C_2H_4OH dissociation cannot be measured, since one OH is formed for every OH radical that reacts. Hence, the overall rate constants that are measured here refer to reactions 12a + 12c (with CH_3CH_2O from 12c in ~5% yield[9] giving CH_3CHO + H), and these constitute ~80% of the total rate constant, with C_2H_4OH formation from reaction 12b being ~20%.

Using a path length of 56 passes (4.9 m), overall rate constants were directly measured between 857 and 1297 K by observing OH decays for the conditions shown in Table S1. Figure 4 shows two typical profiles. Using the reaction mechanism of Table 4, these profiles were simulated giving the lines shown in the figure. Figures 5 and 6 illustrate sensitivity analyses for the experiments shown in Figure 4. Clearly, *t*BH dissociation and reaction 12 are the only important processes that determine the profiles, with all other processes being negligible. This suggests that first-order analyses, at longer times after *t*BH has essentially been depleted, would be adequate with the present high sensitivity for OH detection. This is confirmed in columns 5 and 6 of Table S1, where the fitted profile results are compared with those from first-order analysis. The agreement is within ±8%. An added result from the profile fits is that the $[t\text{BH}]_0$ needed (column 7) for the simulations is (31.6 ± 1.0) mol % × $X_{t\text{BH,sol'n}}$, in excellent agreement with the supplier's assay. Over the T range 857−1297 K, the rate constants from simulated fits can be represented by the Arrhenius expression,

$$k_{12} = (2.5 \pm 0.43) \times 10^{-11} \exp(-911 \pm 191 \text{ K}/T) \text{ cm}^3 \text{ molecule}^{-1} \text{ s}^{-1} \quad (14)$$

The fitted rate constants for reaction 12 have been used to evaluate the high-T (621−1297 K) rate behavior. As argued above, these values refer almost entirely to 12a, since 12c is at most ~5% of the total rate. To evaluate the rate constants for 12a over this range, we have used Hess and Tully's data above 621 K[51] and the present simulated results from Table S1. Between 621 and 1297 K, the rate constants can be represented by the Arrhenius expression

$$k_{12a} = (3.03 \pm 0.16) \times 10^{-11} \exp(-1132 \pm 51 \text{ K}/T) \text{ cm}^3 \text{ molecule}^{-1} \text{ s}^{-1} \quad (15)$$

In the present evaluation, the data point of Bott and Cohen[53] is not included. Hence we use only the values of Hess and Tully and the present determinations, with each given the same statistical weight. At the 1 standard deviation (SD) level, the points from Hess and Tully are within ±1%, whereas those from the present study are within ±5% of the line determined from eq 15.

The present ab initio TST predictions for the rate coefficient for reaction 12a + 12c are compared in Figure 7 with the present and other experimental data[46−58] and the related theoretical predictions of Xu and Lin[9] and of Galano et al.[45] The present theoretical predictions (red solid line) are only slightly higher (~30%) than the present high-temperature experimental measurements. However, as the temperature decreases, the present predictions increasingly overestimate the experimental values. Notably, simply ignoring tunneling (red dotted line) yields theoretical predictions that are in much improved agreement with experiment, but which are now slightly too low at the lowest temperatures. This observation suggests that the asymmetric Eckart formula may simply be overestimating the effect of tunneling for this reaction, which is reasonable. Alternatively, simply increasing each of the abstraction barriers by 0.35 kcal/mol (red dash−dot−dot−dot line) also yields a result that is in satisfactory agreement with experiment throughout the range of experimentally studied temperatures. Such an error of 0.35 kcal/mol is well within the uncertainty in this quantity, which might be roughly estimated as 1 kcal/mol.

The theoretical predictions of Xu and Lin[9] are in better agreement with the present high temperature measurements, but appear to be too low at low temperatures. The latter result is somewhat surprising, given that the barrier of Xu and Lin[9] for the dominant channel, 12a, is 0.5 kcal/mol lower than the one calculated here. However, they do not include tunneling for this channel, and they also appear to employ hindered rotors for only one of the torsional modes. Both of these limitations appear to have a significant effect on the predicted rate coefficients. The nonnegligible effect of tunneling, even though the saddlepoint lies below the reactants, is due to the fact that the barriers for rotationally and vibrationally excited states are still above the threshold for reaction. As a result, tunneling still increases the reactive flux. The predictions of Galano et al.[45] are markedly lower, apparently due to their barrier of 0.4 kcal/mol for channel 12a, which is 0.5 kcal/mol greater than predicted here. For the dissociation experiments to follow, the Xu and Lin[9] theoretical predictions are used in the Table 4 mechanism to extrapolate rate constants for OH + CH_3CH_2OH to somewhat higher T.

The present theoretical predictions for the branching ratios (with each of the barrier heights adjusted up by 0.35 kcal/mol) are compared in Figure 8 with those from Xu and Lin[9] and from Galano et al.[45] All three theoretical studies predict a

TABLE 4: Mechanism for C_2H_5OH Decomposition[a]

1.	$C_2H_5OH \rightarrow C_2H_4 + H_2O$	k_1 = to be fitted	present
2.	$C_2H_5OH \rightarrow CH_3 + CH_2O + H$	k_2 = to be fitted	present
3.	$C_2H_5OH + Kr \rightarrow C_2H_4 + OH + H$	k_3 = to be fitted	present
4.	$H + O_2 \rightarrow OH + O$	$k_4 = 1.62 \times 10^{-10} \exp(-7474\ K/T)$	62
5.	$OH + O \rightarrow O_2 + H$	$k_5 = 5.42 \times 10^{-13} T^{.375} \exp(950\ K/T)$	11, 63, 64
6.	$OH + OH \rightarrow O + H_2O$	$k_6 = 7.19 \times 10^{-21} T^{2.7} \exp(917\ K/T)$	11, 63−65
7.	$OH + H_2 \rightarrow H_2O + H$	$k_7 = 3.56 \times 10^{-16} T^{1.52} \exp(-1736\ K/T)$	66
8.	$HO_2 + Kr \rightarrow H + O_2 + Kr$	$k_8 = 7.614 \times 10^{-10} \exp(-22\ 520\ K/T)$	67
9.	$HO_2 + OH \rightarrow H_2O + O_2$	$k_9 = 5.00 \times 10^{-11}$	68
10.	$OH + H \rightarrow H_2 + O$	$k_{10} = 3.78 \times 10^{-20} T^{2.67} \exp(-2393\ K/T)$	11, 63, 64
11.	$O + H_2 \rightarrow OH + H$	$k_{11} = 8.44 \times 10^{-20} T^{2.67} \exp(-3167\ K/T)$	11
12.	$C_2H_5OH + OH \rightarrow CH_3CHO + OH + H$	$k_{12} = 9.11 \times 10^{-20} T^{2.58} \exp(748\ K/T)$	9
13.	$C_2H_5OH + D \rightarrow CH_3CHO + HD + H$	k_{13} from present adjusted theory	eq 20
14.	$H_2O + H \rightarrow OH + H_2$	$k_{14} = 1.56 \times 10^{-15} T^{1.52} \exp(-9083\ K/T)$	11, 63, 64
15.	$O + H_2O \rightarrow OH + OH$	$k_{15} = 7.48 \times 10^{-20} T^{2.7} \exp(-7323\ K/T)$	11, 63, 64
16	$C_2H_5OH + H \rightarrow CH_3CHO + H_2 + H$	k_{16} from present adjusted theory	eq 20
17.	$C_2H_5OH + O \rightarrow CH_3CHO + OH + H$	$k_{17} = 2.89 \times 10^{-16} T^{1.62} \exp(-1210\ K/T)$	69
18.	$CH_3CHO + OH \rightarrow CH_3 + H_2O + CO$	$k_{18} = 8.36 \times 10^{-11} \exp(-2410\ K/T) + 4.34 \times 10^{-12} \exp(369\ K/T)$	70
19.	$CH_3CHO \rightarrow CH_3 + HCO$	$k_{19} = 4.29 \times 10^{22} T^{-1.88} \exp(-43\ 020\ K/T)$	71
20.	$C_4H_{10}O_2 \rightarrow CH_3 + OH + (CH_3)_2CO$	$k_{20} = 2.5 \times 10^{15} \exp(-21\ 649\ K/T)$	72
21.	$(CH_3)_2CO + OH \rightarrow CH_2COCH_3 + H_2O$	$k_{21} = 4.9 \times 10^{-11} \exp(-2297\ K/T)$	73
22.	$H_2CO + Kr \rightarrow HCO + H + Kr$	$k_{22} = 1.019 \times 10^{-8} \exp(-38\ 706\ K/T)$	74
23.	$H_2CO + Kr \rightarrow H_2 + CO + Kr$	$k_{23} = 4.658 \times 10^{-9} \exp(-32\ 110\ K/T)$	74
24.	$HCO + Kr \rightarrow H + CO + Kr$	$k_{24} = 6.00 \times 10^{-11} \exp(-7722\ K/T)$	75
25.	$H_2CO + OH \rightarrow H_2O + HCO$	$k_{25} = 5.69 \times 10^{-15} T^{1.18} \exp(225\ K/T)$	76
26.	$CH_3 + CH_3 \rightarrow C_2H_6$	$k_{26} = f(\rho, T)$	77
27.	$CH_3 + CH_3 \rightarrow C_2H_4 + 2H$	$k_{27} = 5.26 \times 10^{-11} \exp(-7392\ K/T)$	19
28.	$CH_3 + OH \rightarrow {}^1CH_2 + H_2O$	$k_{28} = 1.80 \times 10^{-11}$	78
29.	$OH + C_2H_4 \rightarrow H_2O + H + C_2H_2$	$k_{29} = 1.02 \times 10^{-9} \exp(-7411\ K/T)$	79
30.	$CH_3 + O \rightarrow H_2CO + H$	$k_{30} = 1.148 \times 10^{-10}$	80, 81
31.	$H_2CO + O \rightarrow OH + HCO$	$k_{31} = 6.92\times 10^{-13} T^{0.57} \exp(-1390\ K/T)$	76
32.	$CH_3 + O \rightarrow H_2 + CO + H$	$k_{32} = 2.52\times 10^{-11}$	80, 81
33.	$C_2H_6 + O \rightarrow OH + H + C_2H_4$	$k_{33} = 1.87 \times 10^{-10} \exp(-7411\ K/T)$	82
34.	$C_2H_6 + OH \rightarrow H_2O + H + C_2H_4$	$k_{34} = 2.68 \times 10^{-18} T^{2.224} \exp(-373\ K/T)$	83
35.	$C_2D_5I \rightarrow C_2D_4 + D + I$	$k_{35} = 2.49 \times 10^{10} \exp(-17\ 729\ K/T) \times (0.3037 + (2.744 \times 10^{-4})T)$	84
36.	$C_2D_5I \rightarrow C_2D_4 + DI$	$k_{36} = 2.49 \times 10^{10} \exp(-17\ 729\ K/T) \times (0.6963 - (2.744 \times 10^{-4})T)$	84
37.	$H + C_2D_4 \rightarrow C_2D_3H + D$	$k_{37} = 3.482 \times 10^{-10} \exp(-2784\ K/T)$	85, 86
38.	$D + CH_3 \rightarrow CH_2D + H$	$k_{38} = 2.20 \times 10^{-10}$	84

[a] All rate constants are in cm^3 molecule^{-1} s^{-1}.

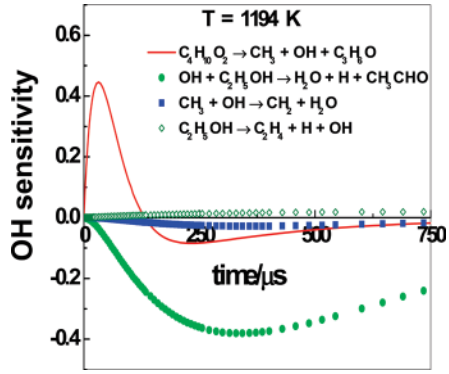

Figure 5. OH radical sensitivity analysis for the 1194 K profile shown in Figure 4 using the full reaction mechanism scheme listed in Table 4 and the modeled rate constants (k_{12}) in Table 4. The four most sensitive reactions are shown in the inset.

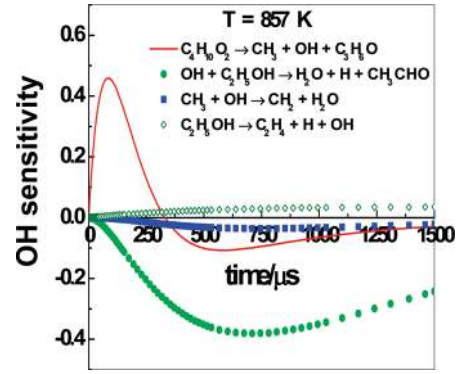

Figure 6. OH radical sensitivity analysis for the 857 K profile shown in Figure 4 using the full reaction mechanism scheme listed in Table 4 and the modeled rate constants (k_{12}) in Table 4. The four most sensitive reactions are shown in the inset.

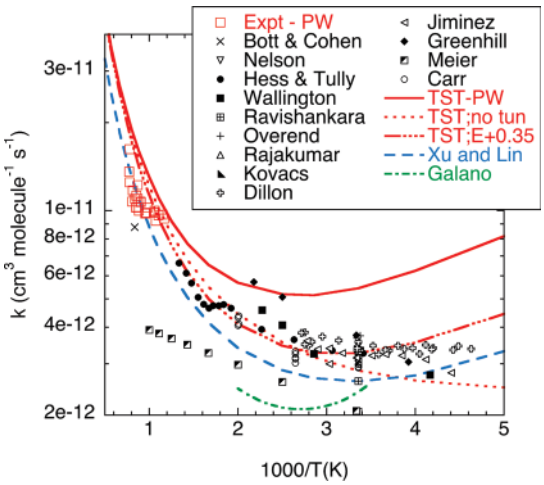

Figure 7. Arrhenius plot of the experimental data (symbols) and theoretical predictions (lines) for the OH + C_2H_5OH rate coefficient. The red symbols denote the present experimental measurements, and the remaining symbols denote other experimental data.[46−58] The red lines denote the present theoretical predictions, with the solid line corresponding to the unadjusted predictions; the dotted line, the predictions when tunneling is neglected; and the dash−dot−dot−dot line, the predictions when the saddle points are shifted up by 0.35 kcal/mol. The blue dashed and green dash−dot lines denote the ab initio TST predictions of Xu and Lin[9] and Galano et al.,[45] respectively.

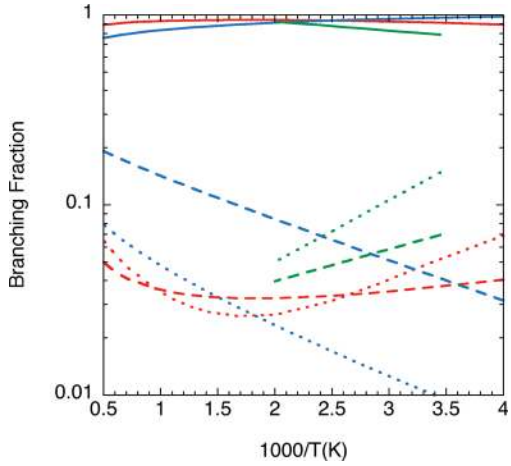

Figure 8. Arrhenius plot of the branching fraction [$k_{12i}/(k_{12a} + k_{12b} + k_{12c})$] for 12i = channels 12a (solid), 12b (dashed), and 12c (dotted). The ab initio TST predictions from the present work with barriers adjusted up by 0.35 kcal/mol are in red, those from Xu and Lin[9] are in blue, and those from Galano et al.[45] are in green.

branching ratio to $CH_3CHOH + H_2O$ of ∼90%, which is in reasonable agreement with Meier et al.'s[48] experimental result of 75 ± 15%. However, the branching to the secondary channels is quite different for the three studies. The present calculations predict a higher branching to channel 12c at low temperature due to a greater imaginary frequency (2432i versus 1335i).

The present adjusted theoretical predictions for the total and channel-specific rate coefficients are well reproduced over the 200−2500 K T range by the expressions

$$k_{12} = 5.02 \times 10^{-20}\, T^{2.67} \exp(844\ \mathrm{K}/T)\ \mathrm{cm^3\ molecule^{-1}\ s^{-1}} \quad (16)$$

$$k_{12a} = 1.19 \times 10^{-19}\, T^{2.54} \exp(772\ \mathrm{K}/T)\ \mathrm{cm^3\ molecule^{-1}\ s^{-1}} \quad (16a)$$

$$k_{12b} = 9.46 \times 10^{-24}\, T^{3.38} \exp(1205\ \mathrm{K}/T)\ \mathrm{cm^3\ molecule^{-1}\ s^{-1}} \quad (16b)$$

$$k_{12c} = 9.64 \times 10^{-27}\, T^{4.28} \exp(1792\ \mathrm{K}/T)\ \mathrm{cm^3\ molecule^{-1}\ s^{-1}} \quad (16c)$$

The sum of these three parameter fits for k_{12a} and k_{12c} is within ±30% of eq 15 over the T range 621−1297 K.

D + CH_3CH_2OH. As with H-atom abstractions by OH, a theoretical study by Park et al.[10] on H + C_2H_5OH predicts contribution from only three channels over a wide temperature range,

$$\mathrm{H + CH_3CH_2OH \rightarrow products} \quad (17)$$

$$\rightarrow \mathrm{CH_3CHOH + H_2} \quad (17a)$$

$$\rightarrow \mathrm{CH_2CH_2OH + H_2} \quad (17b)$$

$$\rightarrow \mathrm{CH_3CH_2O + H_2} \quad (17c)$$

with 17c being a minor process (∼5%) over the T range 298−3000 K. If C_2H_5I were to be used as a thermal source for H-atoms in H + C_2H_5OH experiments, then the additional production of H-atoms from the thermal decomposition of C_2H_5OH would be a potential complication. Instead, we have performed D + C_2H_5OH experiments using C_2D_5I as a thermal source for D-atoms. With this source and the observation of D-atom time-dependent concentrations, the secondary production of H-atoms no longer interferes with the observation. Channels analogous to 17a−c are expected to occur in the deuterated case (see below), and we have therefore utilized theoretical calculations to gauge the isotope effect as discussed below and in the preceding theory section.

$$\mathrm{D + CH_3CH_2OH \rightarrow products} \quad (18)$$

$$\rightarrow \mathrm{CH_3CHOH + HD} \quad (18a)$$

$$\rightarrow \mathrm{CH_2CH_2OH + HD} \quad (18b)$$

$$\rightarrow \mathrm{CH_3CH_2O + HD} \quad (18c)$$

Seventeen experiments were performed over the T range 1054−1359 K to obtain total rate constants for reaction 18. Table S2 gives the experimental conditions and summarizes the measured rate constants. Figure 9 is an example of a typical D-atom profile obtained at 1159 K. The D-atom profile is simulated using the model in Table 4 to obtain the total bimolecular rate constant for reaction 18. Both Park et al.[10] and the present ab initio TST calculations predict that >75% of the abstraction occurs through channel 17a at T < 1400 K, and therefore, for the purpose of modeling the experiments, we have used only reaction 18a. Figure 10 shows the sensitivity analysis for the D-atom profile of Figure 9. Clearly, C_2D_5I dissociation and the title reaction are the only sensitive reactions with the long-time D-atom tail governed by H + $C_2D_4 \rightarrow C_2D_3H$ + D.

The present ab initio TST calculations predict that the rate coefficient for reaction 18 is within 5% of that for reaction 17 over the T range 1054−1359 K (i.e., an isotope effect of ∼1.0).

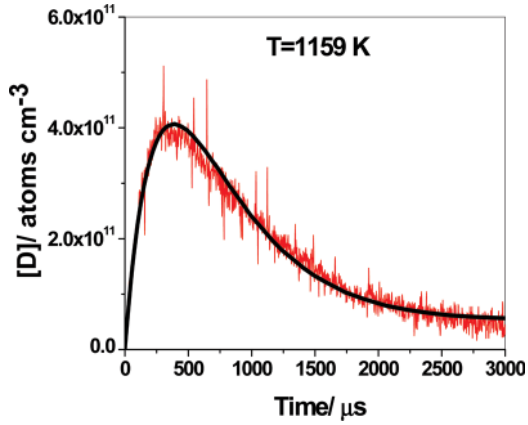

Figure 9. [D] profile at 1159 K. The solid line is a fit over the entire time range using the reaction mechanism of Table 4 with the k_{13} values from Table S2. The conditions for the experiment at 1159 K are $P_1 = 15.94$ Torr, $M_s = 2.105$, $\rho_5 = 2.520 \times 10^{18}$ molecules cm^{-3}, $[C_2D_5I]_0 = 1.28 \times 10^{12}$ molecules cm^{-3}, and $[C_2H_5OH]_0 = 2.18 \times 10^{14}$ molecules cm^{-3}.

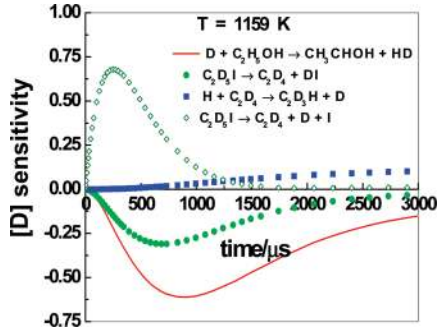

Figure 10. D-atom sensitivity analysis for the 1159 K profile shown in Figure 4 using the full reaction mechanism scheme listed in Table 4 with the k_{13} value in Table S2. The four most sensitive reactions are shown in the inset.

Thus, we consider the present measurement to relate directly to reaction 17. Over the T range 1054−1359 K, the rate constants from simulated fits can be represented by the Arrhenius expression,

$$k_{16} = (3.98 \pm 0.76) \times 10^{-10} \exp(-4494 \pm 235\ \mathrm{K}/T)\ \mathrm{cm}^3\ \mathrm{molecule}^{-1}\ \mathrm{s}^{-1} \quad (19)$$

At the 1 SD level, the present experimental data are within ±19% of eq 19. The present experiments and the lower temperature (295−473 K) measurements of Aders and Wagner[59] are the only direct measurements for this rate constant.

As shown in Figure 11, the present theoretical predictions for k_{16} are in reasonable agreement with the present experiments, being ∼40% higher. The prior ab initio TST calculations of Park et al.[10] differ by a similar magnitude, but are instead ∼50% lower. There are similar differences between the theoretical predictions and the experimental results of Aders and Wagner.[59] Repeating the present TST calculations with each of the barriers increased by 0.8 kcal/mol (which is within the uncertainty of the ab initio electronic structure calculations) yields results that accurately reproduce both the present experimental results and those from ref 59. These adjusted ab initio TST rate coefficients

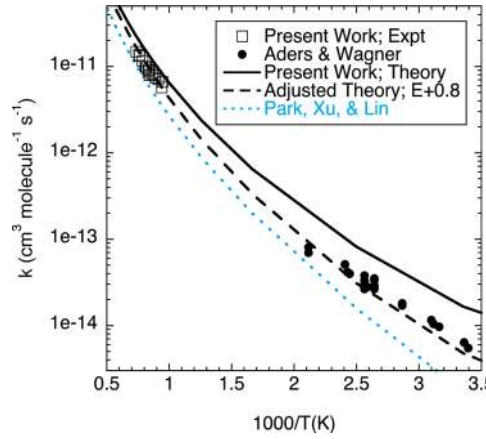

Figure 11. Arrhenius plot of the experimental data (symbols) and theoretical predictions (lines) for the H/D + C_2H_5OH rate coefficients. The open squares denote the present experimental measurements of the total rate coefficient, and the circles denote those from ref 59. The black solid and dashed lines denote the present theoretical predictions before and after the adjustment of the barrier by 0.8 kcal/mol. The blue dotted line denotes the theoretical predictions from Park et al.[10]

are well reproduced over the 300−2250 K T range by the following modified Arrhenius expressions:

$$k_{16} = 1.85 \times 10^{-21} T^{3.30} \exp(-1214\ \mathrm{K}/T)\ \mathrm{cm}^3\ \mathrm{molecule}^{-1}\ \mathrm{s}^{-1} \quad (20)$$

$$k_{16a} = 1.46 \times 10^{-19} T^{2.68} \exp(-1467\ \mathrm{K}/T)\ \mathrm{cm}^3\ \mathrm{molecule}^{-1}\ \mathrm{s}^{-1} \quad (20a)$$

$$k_{16b} = 8.82 \times 10^{-20} T^{2.81} \exp(-3772\ \mathrm{K}/T)\ \mathrm{cm}^3\ \mathrm{molecule}^{-1}\ \mathrm{s}^{-1} \quad (20b)$$

$$k_{16c} = 1.57 \times 10^{-21} T^{3.14} \exp(-4379\ \mathrm{K}/T)\ \mathrm{cm}^3\ \mathrm{molecule}^{-1}\ \mathrm{s}^{-1} \quad (20c)$$

The branching between the channels is similar to what was predicted by Park et al.,[10] with channel 20a being the dominant channel. Channel 20b is predicted to be a significant secondary channel, with a fraction that increases with increasing temperature, reaching 38% at 2500 K. However, channel 20c is essentially negligible with a maximum fraction of 7% at 2500 K.

CH_3CH_2OH Dissociation. Using the same OH radical detection method, we have directly measured the rate of formation of OH from ethanol dissociation, and this can be attributed directly to reaction 3. Figure 12 shows a typical example of a profile at 1555 K. The profiles exhibit considerable scatter, but the initial slopes can be used to determine k_3 by modeling using the mechanism in Table 4. A first order rise time constant for $k_3 = 100$ s^{-1} in the Table 4 mechanism represents the best fit to the OH profile. Note that the level of OH detected is ∼5−7 × 10^{12} radicals cm^{-3} at a signal-to-noise ratio of ∼3. To our knowledge, this level of sensitivity for $[OH]_t$ in shock wave experiments has never been exceeded before. The experimental conditions and k_3 results are given in Table S3, and a first-order plot is shown in Figure 13. Because of the limited data set and scatter, only a minor P dependence is suggested by the experiments. With the substantial data scatter,

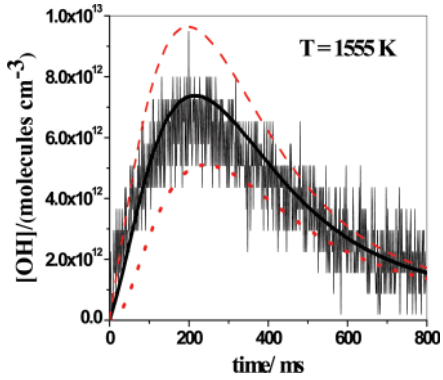

Figure 12. [OH] profile at 1555 K for an ethanol dissociation experiment. The conditions for the experiment at 1555 K are P_1 = 10.89 Torr, M_s = 2.479, $\rho_5 = 2.051 \times 10^{18}$ molecules cm^{-3}, and $[C_2H_5OH]_0 = 4.63 \times 10^{14}$ molecules cm^{-3}. Solid line, $k_3 = 100$ s^{-1} in Table 4 mechanism; dotted line, $k_3 = 0$ s^{-1} in Table 4 mechanism; dashed line, $k_3 = 200$ s^{-1} in Table 4 mechanism.

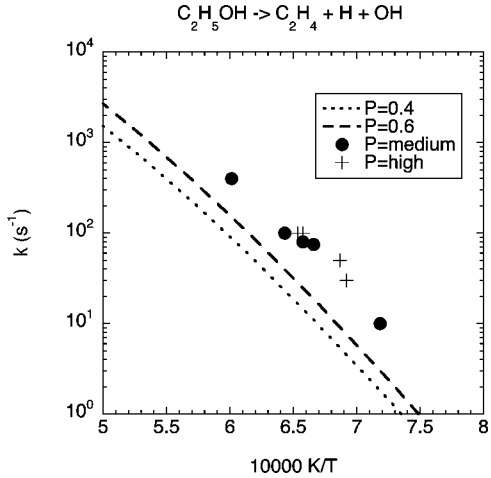

Figure 13. Arrhenius plot of the data for k_3 over the T range, 1392−1663 K. ●, +: data from present work at medium and high pressures, respectively, Table S3. Dashed and dotted line: theory from present work at pressures of 0.4 and 0.6 atm, respectively, which correlate with the medium and high experimental pressures.

the fitted results are not particularly accurate but can be expressed by the second-order expression

$$k_3 = (3.68 \pm 1.93) \times 10^{-12} \exp(-16\,586 \pm 1143\ \mathrm{K}/T)\ \mathrm{cm^3\ molecule^{-1}\ s^{-1}} \quad (21)$$

Figure 13 also shows the present theoretical predictions for the two representative experimental data sets at 0.4 and 0.6 atm. Over the T range of overlap, the theoretical predictions are a factor of ∼5 lower than the experiments. Given the fact that this is a higher-lying minor channel, which is very sensitive to energy transfer, and taking into account the scatter in the experiments, we think the agreement between experiment and theory is reasonable.

Using H-atom ARAS, ethanol dissociation experiments have been performed as a function of both pressure and temperature. Figure 14 shows two H-atom profiles in which maximum [H] is ∼1−2 × 10^{12} atoms cm^{-3} with a signal-to-noise ratio of ∼10. H-atoms are formed from the fast dissociations of the CH_2OH and C_2H_5 radicals that are products of reactions 2 and 3, respectively.

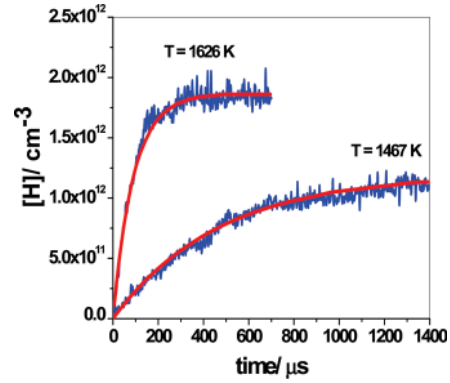

Figure 14. Two [H] profiles at 1626 and 1457 K, respectively. The solid lines are fits over the entire time range using the reaction mechanism of Table 4 with the k_1 and k_2 values from Table S4. The conditions for the experiment at 1626 K are P_1 = 15.97 Torr, M_s = 2.557, $\rho_5 = 3.109 \times 10^{18}$ molecules cm^{-3}, and $[C_2H_5OH]_0 = 3.19 \times 10^{12}$ molecules cm^{-3}. The conditions for the experiment at 1457 K are P_1 = 5.71 Torr, M_s = 2.403, $\rho_5 = 1.051 \times 10^{18}$ molecules cm^{-3}, and $[C_2H_5OH]_0 = 2.46 \times 10^{12}$ molecules cm^{-3}.

Since the detectability for [H] is so low, the effects of secondary reactions involving H are negligible. This means that first-order analysis should be sufficient; that is, $[H]_t$ should be affected only by the three dissociation processes. Hence, the present results are a direct measure of dissociation. First-order analysis gives the simple closed form result

$$[H]_t = \{(k_2 + k_3)[C_2H_5OH]_0/(k_1 + k_2 + k_3)\} \times \{1 - \exp(-(k_1 + k_2 + k_3)t)\} \quad (22)$$

where $[H]_\infty = (k_2 + k_3)[C_2H_5OH]_0/(k_1 + k_2 + k_3)$, $BR_{2,3} = (k_2 + k_3)/(k_1 + k_2 + k_3)$ (branching ratio to 2 and 3), and $BR_1 = 1 - BR_{2,3}$. Rough values, for initially estimating total decomposition rate constants, were obtained from first-order build-up plots of $\ln\{([H]_\infty - [H]_t)/[H]_\infty\}$ against time. The theoretical predictions for k_3 were scaled by a factor of 5 (to match experiment), and subsequently, $BR_{2,3}$ and k_{total} (i.e., $k_1 + k_2 + k_3$) were systematically varied until the simulations matched experiments. The lines in Figure 14 are simulations using the mechanism in Table 4, with k_1 and k_2 determined from eq 22 and the predetermined k_3 (theory scaled by 5). For the present range of conditions, the three quantities obtained from eq 22 were within ±5% of those determined from the complete mechanistic simulations, confirming our conclusion that the results are direct and not substantially perturbed by secondary reactions. We subsequently have used the first-order analytical method to fit the entire set of experiments listed in Table S4. Figures 15 and 16 show corresponding sensitivity analyses for the two experiments. Clearly, the predominant reactions that determine $[H]_t$ are 1, 2, and 3, with 3 already being taken into account. The conditions for these experiments and the resulting first-order values for k_1, k_2, and $BR_{2,3}$ are also given in the table (S4).

As noted in the Theory section, the present a priori theoretical predictions appear to significantly underestimate the rate coefficient k_1, particularly at low temperatures. Decreasing the barrier height for this channel by 2 kcal/mol yields quantitative agreement with the experiments of Li et al.[3] and of Herzler et al.[5] However, a reduction by 2 kcal/mol would be somewhat outside the expected uncertainty limits of the theoretical analysis. Furthermore, reproducing the present experimental results then requires energy transfer rates that are lower than typical. In particular, an optimal fit for the total rate constant requires

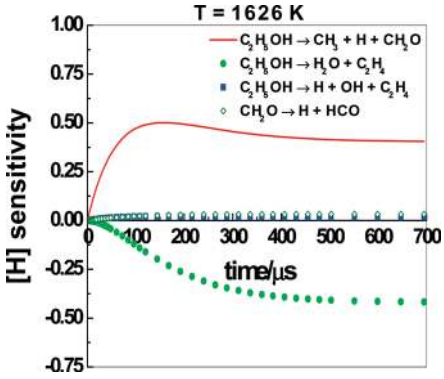

Figure 15. H-atom sensitivity analysis for the 1626 K profile shown in Figure 14 using the full reaction mechanism scheme listed in Table 4 with k_1 and k_2 values in Table S4. The four most sensitive reactions are shown in the inset.

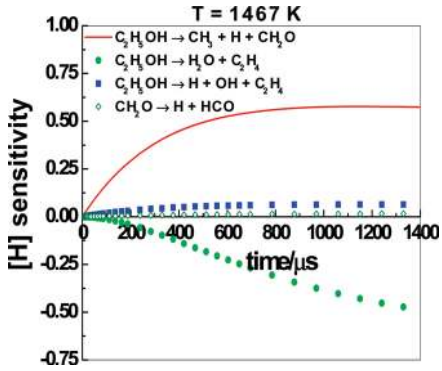

Figure 16. H-atom sensitivity analysis for the 1457 K profile shown in Figure 14 using the full reaction mechanism scheme listed in Table 4 with k_1 and k_2 values in Table S4. The four most sensitive reactions are shown in the inset.

setting $\langle \Delta E_{down} \rangle$ to 50 $(T/300)^{0.85}$ cm^{-1}, whereas prefactors of 100−200 cm^{-1} are more typical. Even more problematic is that such small energy transfer rates yield rate coefficients for channels 2 and 3 that are an order of magnitude too low.

At the temperature and pressures of the present experiments, the rate coefficients for channels 2 and 3 are very sensitive to both the energy transfer parameters and the height of the barrier to channel 1, since their production involves a competition between dissociation to channel 1 and further excitation. A compromise fit to all the data is obtained by lowering the barrier to channel 1 by only 1.0 kcal/mol, and setting $\langle \Delta E_{down} \rangle$ to 125 $(T/300)^{0.85}$ cm^{-1}. With this compromise, a reasonably satisfactory reproduction of all the experimental data is obtained. Furthermore, this reduced adjustment of the barrier is within the expected uncertainty of the electronic structure evaluations, and this expression for $\langle \Delta E_{down} \rangle$ is typical of those found in other related studies.

The present experimental measurements for k_1, k_2, and k_3 are plotted as first-order rate constants together with these adjusted and optimized theoretical predictions in Figures 17, 18, and 13, respectively. The corresponding experimental and theoretical branching ratios are plotted in Figure 19. In each of these plots, the theoretical predictions are for pressures of 0.2, 0.4, 0.6, and 1.0 atm for comparison with the experimental measurements labeled low, medium, high, and higher, which span a small range of pressures centered as these values.

The theoretical predictions for k_1 pass through the mean of the present experimental measurements, with a pressure variation that more or less matches that observed experimentally. They are, however, about a factor of 1.5−2.5 lower than the

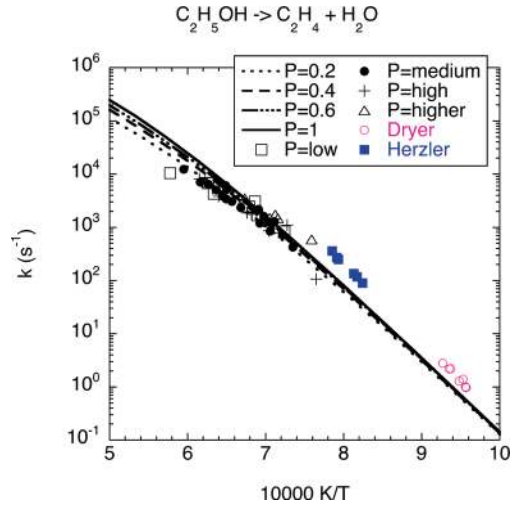

Figure 17. Arrhenius plot of the data for k_1 over the T range, 1308−1732 K. □, 0.20−0.28 atm expt present work; ●, 0.36−0.50 atm expt present work; +, 0.49−0.69 atm expt present work; Δ, 0.95−1.28 atm expt present work. Dotted, dashed, dash−dot−dot−dot, and solid lines: theory from present work for pressures of 0.2, 0.4, 0.6, and 1.0 atm, respectively.

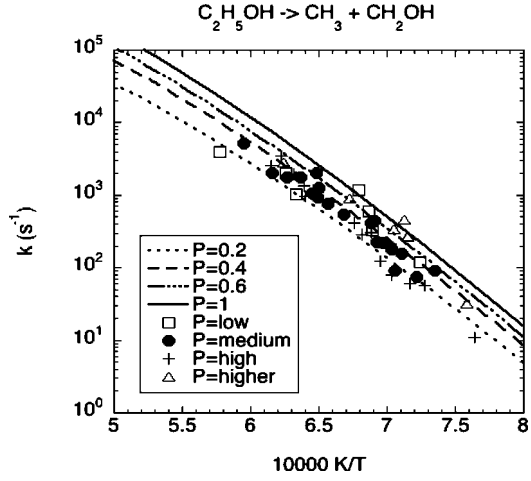

Figure 18. Arrhenius plot of the data for k_2 over the T range 1308−1732 K. Symbols and lines as in Figure 17.

measurements of Li et al.[3] and Herzler et al.[5] The theoretical predictions for k_2 also pass through the mean of the present experimental measurements and with a pressure variation that more or less matches that observed experimentally. The theoretical predictions for k_3 are somewhat lower than the experimental measurements, but are still generally within a factor of 4. As noted earlier, this discrepancy seems reasonable, given the difficulty of measuring the rate coefficient for the low branching to this channel (recall the need to fit just the rise in the OH profiles rather than their full time dependence) and the strong sensitivity of the theoretical predictions to the details of the energy transfer process (some contribution from strong collisions might greatly enhance the rate through this pathway).

The present adjusted predictions for the temperature dependence of k_1, k_2, and k_3 have been fitted with modified Arrhenius expressions for a wide range of pressures. These expressions are summarized in Table 5. Also included in Table 5 are modified Arrhenius expressions for the high-pressure limits of the rate coefficients for the $CH_3 + CH_2OH$ and $C_2H_5 + OH$ recombinations. These predictions for the high pressure recombination rate coefficients are each ∼1.5 times lower than the corresponding room temperature experimental measurements of

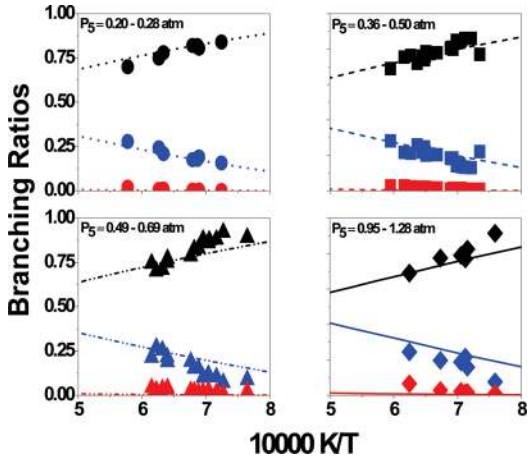

Figure 19. Branching ratios for the three ethanol dissociation channels over the T range 1308−1732 K. ●, 0.20−0.28 atm expt present work; ■, 0.36−0.50 atm expt present work; ▲, 0.49−0.69 atm expt present work; ♦, 0.95−1.28 atm expt present work. Dotted lines, 0.2 atm theory present work; dashed lines, 0.4 atm theory present work; dash-dot-dot-dot lines, 0.6 atm theory present work; solid line, 1 atm theory present work. Black symbols and lines represent $BR_1 = k_1/(k_1 + k_2 + k_3)$, blue symbols and lines represent $BR_2 = k_2/(k_1 + k_2 + k_3)$, red symbols and lines represent $BR_3 = k_3/(k_1 + k_2 + k_3)$.

TABLE 5: Modified Arrhenius Expressions[a] for Rate Coefficients in the Decomposition of C_2H_5OH

pressure (atm)	A (s^{-1})[b]	n	E_0 (K)
	$C_2H_5OH \rightarrow C_2H_4 + H_2O$[c]		
0.001	3.41×10^{59}	−14.22	42 110
0.01	2.62×10^{57}	−13.29	42 910
0.1	1.65×10^{52}	−11.52	42 650
1	5.23×10^{43}	−8.90	41 020
10	4.59×10^{32}	−5.60	38 280
100	3.84×10^{20}	−2.06	34 960
	$C_2H_5OH \rightarrow CH_3 + CH_2OH$[c]		
0.001	1.20×10^{54}	−12.94	50 330
0.01	5.18×10^{59}	−13.98	50 280
0.1	1.62×10^{66}	−15.30	53 040
1	5.55×10^{64}	−14.47	53 900
10	1.55×10^{58}	−12.29	53 230
100	1.78×10^{47}	−8.96	50 860
	$C_2H_5OH \rightarrow C_2H_5 + OH$[c]		
0.001	8.10×10^{46}	−11.33	55 890
0.01	1.82×10^{56}	−13.49	53 970
0.1	4.65×10^{63}	−14.99	55 170
1	1.46×10^{65}	−14.89	56 540
10	2.79×10^{61}	−13.40	56 910
100	6.17×10^{51}	−10.34	55 330
	$C_2H_5 + OH \rightarrow C_2H_5OH$[d]		
infinity	2.65×10^{-9}	−0.609	−38.4
	$CH_3 + CH_2OH \rightarrow C_2H_5OH$[d]		
infinity	2.77×10^{-10}	−0.189	22.9

[a] Rate coefficient $= A\ T^n \exp(-E_0/T)$, where T is in K. [b] For the $C_2H_5 + OH \rightarrow C_2H_5OH$ and $CH_3 + CH_2OH \rightarrow C_2H_5OH$ reactions, the parameter A has units of cm^3 $molecule^{-1}$ s^{-1}. [c] Valid over the T range 800−2000 K. [d] Valid over the T range 200−2000 K.

Pagsberg et al.[60] for the $CH_3 + CH_2OH$ reaction and of Fagerstrom et al.[61] for the $C_2H_5 + OH$ reaction.

In Figures 20−22, the present theoretical predictions are contrasted with the related ab initio TST-based master equation simulations from Park et al.[10] and Li et al.[3] In each case, there are significant differences between the various theoretical predictions. For k_1, the low-T predictions of Li et al. are higher because they were specifically adjusted to reproduce the

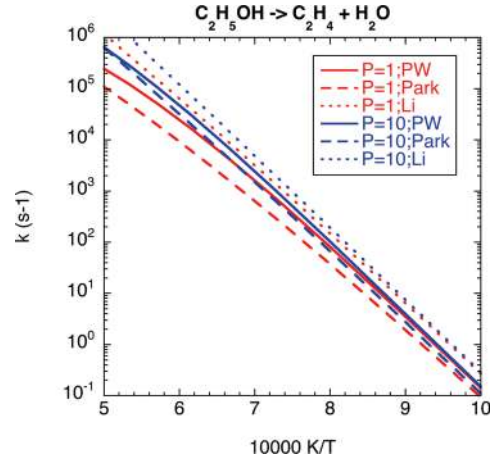

Figure 20. Arrhenius plot of the theoretical predictions for the rate coefficient k_1. The solid, dashed, and dotted lines represent the present theory, the theory of Park et al.,[10] and that of Li et al.,[3] respectively. The red and blue lines denote results for pressures of 1 and 10 atm, respectively.

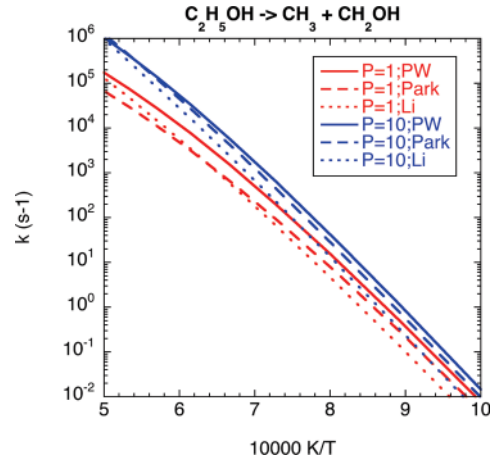

Figure 21. Arrhenius plot of the theoretical predictions for the rate coefficient k_2. The solid, dashed, and dotted lines represent the present theory, the theory of Park et al.,[10] and that of Li et al.,[3] respectively. The red and blue lines denote results for pressures of 1 and 10 atm, respectively.

experimental data from that work. Those adjustments included an unphysical lowering of the two lowest transition state frequencies by about a factor of 2. Regarding the predictions of Park et al., their k_1 values appear to fall off too quickly, especially for the higher temperatures.

For k_2, the treatment of the barrierless potential by Park and co-workers is inadequate both in the methods used to explore it and in the simplifications used to obtain a global representation. In addition, Li et al. simply estimate the high-pressure rate coefficient for this channel from comparison with related reactions. Hence, the observed discrepancies of a factor of 2 or more are to be expected. Similar comments apply to the treatment of k_3 by Park and co-workers, in which large discrepancies are again observed at low pressure. For simplicity, Li et al. did not consider this channel.

Conclusion

The thermal decomposition of ethanol and its reactions with OH and H/D have been studied with both shock tube experiments and ab initio transition state theory-based master equation calculations. Dissociation rate constants for ethanol have been measured at high T in reflected shock waves using OH optical

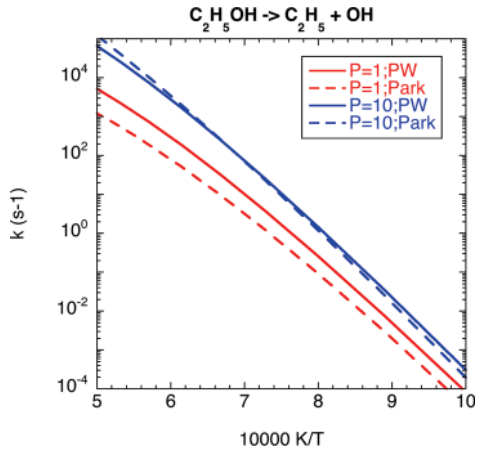

Figure 22. Arrhenius plot of the theoretical predictions for the rate coefficient k_3. The solid and dashed lines represent the present theory and the theory of Park et al.,[10] respectively. The red and blue lines denote results for pressures of 1 and 10 atm, respectively.

absorption and high-sensitivity H-atom ARAS detection. The present theoretical predictions are in good agreement with the experimental data for the three kinetically relevant dissociation channels.

OH optical absorption using the multipass cell was also used to study the reaction of OH with ethanol using *tert*-butyl hydroperoxide (*t*BH) as the thermal source for OH. The present experiments can be represented by the Arrhenius expression

$$k = (2.5 \pm 0.43) \times 10^{-11} \exp(-911 \pm 191\ \mathrm{K}/T)\ \mathrm{cm^3\ molecule^{-1}\ s^{-1}}$$

over the T range 857−1297 K. The theoretical predictions for this abstraction reaction are in good agreement with the available experimental database, including the present high-T experiments.

D-atom ARAS was used to study the reaction of D with ethanol, and the rate constants from the present experiments can be represented by the Arrhenius expression,

$$k = (3.98 \pm 0.76) \times 10^{-10} \exp(-4494 \pm 235\ \mathrm{K}/T)\ \mathrm{cm^3\ molecule^{-1}\ s^{-1}}$$

over the T range 1054−1359 K. The present theory indicates that the isotope effect is minor at high T (>1000 K), and consequently, the present experiments represent a direct measurement of the rate constants for H + C_2H_5OH → products. The theoretical predictions for this reaction are in excellent agreement with the present experiments. The predicted reaction exo- and endothermicities are in good agreement with the current Active Thermochemical Tables values.

The present experimental and theoretical studies on the primary thermal decomposition channels in ethanol and the major abstraction channels involving H and OH now provide a better description of the high T combustion reactions of ethanol, and we recommend the present results for use in combustion modeling.

Acknowledgment. This work was supported by the U.S. Department of Energy, Office of Basic Energy Sciences, Division of Chemical Sciences, Geosciences, and Biosciences, under Contract no. DE-AC02-06CH11357.

Supporting Information Available: Tables of experimental data (S1−S4) have been provided as Supporting Information. This material is available free of charge via the Internet at http://pubs.acs.org.

References and Notes

(1) Marinov, N. M. *Int. J. Chem. Kinet.* **1999**, *31*, 183.
(2) Park, J.; Zhu, R. S.; Lin, M. C. *J. Chem. Phys.* **2002**, *117*, 3224.
(3) Li, J.; Kazakov, A.; Dryer, F. L. *J. Phys. Chem. A* **2004**, *108*, 7671.
(4) Tsang, W. *Int. J. Chem. Kinet.* **2004**, *36*, 456.
(5) Herzler, J.; Manion, J. A.; Tsang, W. *J. Phys. Chem. A* **1997**, *101*, 5500.
(6) Park, J.; Chen, R.; Chen, J.; Lin, M. C. *Experimental and Computational Studies of the Unimolecular Decomposition of Ethanol*. Presented at the Eastern States Section Fall Technical Meeting of the Combustion Institute, Hilton Head, SC, 2001, p 187.
(7) Klippenstein, S. J. *J. Chem. Phys.* **1992**, *96*, 367.
(8) Georgievskii, Y.; Klippenstein, S. J. *J. Phys. Chem. A* **2003**, *107*, 9776.
(9) Xu, S.; Lin, M. C. *Proc. Combust. Inst.* **2007**, *31*, 159.
(10) Park, J.; Xu, Z. F.; Lin, M. C. *J. Chem. Phys.* **2003**, *118*, 9990.
(11) Michael, J. V. *Prog. Energy Combust. Sci.* **1992**, *18*, 327.
(12) Michael, J. V. In *Advances in Chemical Kinetics and Dynamics* Barker, J. R., Ed.; JAI: Greenwich, 1992, Vol. I, pp 47−112; for original references.
(13) Michael, J. V.; Sutherland, J. W. *Int. J. Chem. Kinet.* **1986**, *18*, 409.
(14) Michael, J. V. *J. Chem. Phys.* **1989**, *90*, 189.
(15) Michael, J. V.; Fisher, J. R. In *Seventeenth International Symposium on Shock Waves and Shock Tubes*; Kim, Y. W., Ed.; AIP Conference Proceedings 208; American Institute of Physics: New York, 1990, pp 210−215.
(16) Su, M.-C.; Kumaran, S. S.; Lim, K. P.; Michael, J. V. *Rev. Sci. Instrum.* **1995**, *66*, 4649.
(17) Su, M.-C.; Kumaran, S. S.; Lim, K. P.; Michael, J. V.; Wagner, A. F.; Harding, L. B.; Fang, D.-C. *J. Phys. Chem. A* **2002**, *106*, 8261.
(18) Srinivasan, N. K.; Su, M.-C.; Sutherland, J. W.; Michael, J. V. *J. Phys. Chem. A* **2005**, *109*, 1857.
(19) Lim, K. P.; Michael, J. V. *Proc. Comb. Inst.* **1994**, *25*, 713, and references therein.
(20) Kumaran, S. S.; Su, M.-C.; Lim, K. P.; Michael, J. V. *Proc. Comb. Inst.* **1996**, *26*, 605.
(21) Michael, J. V.; Lifshitz, A. *Handbook of Shock Waves*, Ben-Dor, G., Igra, O., Elperin, T., Lifshitz, A., Eds.; Academic Press: New York, 2001; Vol. 3; pp 77−105.
(22) Srinivasan, N. K.; Su, M.-C.; Michael, J. V. *J. Phys. Chem. A* **2007**, *111*, 3951.
(23) Curtiss, L. A.; Raghavachari, K.; Redfern, P. C.; Rassolov, V.; Pople, J. A. *J. Chem. Phys.* **1998**, *109*, 7764.
(24) Dunning, T. H., Jr. *J. Chem. Phys.* **1989**, *90*, 1007.
(25) Kendall, R. A.; Dunning, T. H., Jr.; Harrison, R. J. *J. Chem. Phys.* **1992**, *96*, 6796.
(26) Becke, A. D. *J. Chem. Phys.* **1993**, *98*, 5648.
(27) Werner, H.-J. *Mol. Phys.* **1996**, *89*, 845.
(28) Celani, P.; Werner, H.-J. *J. Chem. Phys.* **2000**, *112*, 5546.
(29) Lee, T. J.; Taylor, P. R. *Int. J. Quantum Chem.* **1989**, *23*, 199.
(30) Mebel, A. M.; Morkuma, K.; Lin, M. C. *J. Chem. Phys.* **1995**, *103*, 7414.
(31) Baboul, A. G.; Curtiss, L. A.; Redfern, P. C.; Raghavachari, K. *J. Chem. Phys.* **1999**, *110*, 7650.
(32) Ochterski, J. W.; Petersson, G. A.; Montgomery, J. A. *J. Chem. Phys.* **1996**, *104*, 2598. (a) Montgomery, J. A.; Ochterski, J. W.; Petersson, G. A. *J. Chem. Phys.* **1994**, *101*, 5900.
(33) Ruscic, B.; Pinzon, R. E.; Morton, M. L.; von Laszewski, G.; Bittner, S.; Nijsure, S. G.; Amin, K. A.; Minkoff, M.; Wagner, A. F. *J. Phys. Chem. A* **2004**, *108*, 9979. (a) Ruscic, B.; Pinzon, R. E.; von Laszewski, G.; Kodeboyina, D.; Burcat, A.; Leahy, D.; Montoya, D.; Wagner, A. F. *J. Phys. Conf. Ser.* **2005**, *16*, 561.
(34) Ruscic, B.; Pinzon, R. E.; Morton, M. L.; Srinivasan, N. K.; Su, M.-C.; Sutherland, J. W.; Michael, J. V. *J. Phys. Chem. A* **2006**, *110*, 6592. (a) Widicus Weaver, S. L.; Woon, D. E.; Ruscic, B.; McCall, B. J. *Astrophys. J.* **2009**, *697*, 601. (b) Stevens, W. R.; Ruscic, B.; Baer, T. submitted.
(35) Townsend, D.; Lahankar, S. A.; Lee, S. K.; Chambreau, S. D.; Suits, A. G.; Zhang, X.; Rheinecker, J.; Harding, L. B.; Bowman, J. M. *Science* **2004**, *306*, 1158.
(36) Sivaramakrishnan, R.; Michael, J. V.; Klippenstein, S. J. *J. Phys. Chem. A* **2010**, *114*, 755.
(37) Harding, L. B.; Georgievskii, Y.; Klippenstein, S. J. *J. Phys. Chem. A* **2010**, *114*, 765.
(38) Miller, J. A.; Klippenstein, S. J.; Raffy, C. *J. Phys. Chem. A* **2002**, *106*, 4904.

(39) Miller, J. A.; Klippenstein, S. J. *J. Phys. Chem. A* **2006**, *110*, 10528.
(40) Jasper, A. W.; Klippenstein, S. J.; Harding, L. B.; Ruscic, B. *J. Phys. Chem. A* **2007**, *111*, 3932.
(41) Klippenstein, S. J.; Georgievskii, Y.; Harding, L. B. *Phys. Chem. Chem. Phys.* **2006**, *8*, 1133.
(42) *MRCC, a string-based quantum chemical program suite*; written by Kállay, M. (a) See also Kállay, M.; Surján, P. R. *J. Chem. Phys.* **2001**, *115*, 2945.
(43) Kállay, M.; Gauss, J. *J. Chem. Phys.* **2005**, *123*, 214105.
(44) Woon, D. E.; Dunning, T. H. *J. Chem. Phys.* **1995**, *103*, 4572.
(45) Galano, A.; Alvarez-Idaboy, J. R.; Bravo-Perez, G.; Ruiz-Santoyo, M. E. *Phys. Chem. Chem. Phys.* **2002**, *4*, 4648.
(46) Overend, R.; Paraskevopoulos, G. *J. Phys. Chem.* **1978**, *82*, 1379.
(47) Ravishankara, A. R.; Davis, D. D. *J. Phys. Chem.* **1978**, *82*, 2852.
(48) Meier, U.; Grotheer, H.-H.; Riekert, G.; Just, Th. *Chem. Phys. Lett.* **1985**, *115*, 221; *Chem. Phys. Lett.* **1987**, *133*, 162.
(49) Greenhill, P. G.; O'Grady, B. V. *Aust. J. Chem.* **1986**, *39*, 1775.
(50) Wallington, T. J.; Kurylo, M. J. *Int. J. Chem. Kinet.* **1987**, *19*, 1015.
(51) Hess, W. P.; Tully, F. P. *Chem. Phys. Lett.* **1988**, *152*, 183.
(52) Nelson, L.; Rattigan, O.; Neavyn, R.; Sidebottom, H.; Treacy, J.; Nielsen, O. J. *Int. J. Chem. Kinet.* **1990**, *22*, 1111.
(53) Bott, J. F.; Cohen, N. *Int. J. Chem. Kinet.* **1991**, *23*, 1075.
(54) Jimenez, E.; Gilles, M. K.; Ravishankara, A. R. *J. Photochem. Photobiol., A* **2003**, *157*, 237.
(55) Dillon, T. J.; Holscher, D.; Sivakumaran, V.; Horowitz, A.; Crowley, J. N. *Phys. Chem. Chem. Phys.* **2005**, *7*, 249.
(56) Rajakumar, B.; Burkholder, J. B.; Portmann, R. W.; Ravishankara, A. R. *Phys. Chem. Chem. Phys.* **2005**, *7*, 2498.
(57) Kovacs, G.; Szasz-Vadasz, T.; Papadimitriou, V. C.; Dobe, S.; Berces, T.; Marta, F. *React. Kinet. Catal. Lett.* **2005**, *87*, 129.
(58) Carr, S. A.; Baeza-Romero, M. T.; Blitz, M. A.; Price, B. J. S.; Seakins, P. W. *Int. J. Chem. Kinet.* **2008**, *40*, 504.
(59) Von Aders, W.-K.; Wagner, H. G. *Ber. Bunsenges. Phys. Chem.* **1973**, *77*, 712.
(60) Pagsberg, P.; Munke, J.; Sillesen, A.; Anastasi, C. *Chem. Phys. Lett.* **1988**, *146*, 375.
(61) Fagerstrom, K.; Lund, A.; Mahmoud, G.; Jodkowski, J. T.; Ratajaczak, E. *Chem. Phys. Lett.* **1993**, *208*, 321.
(62) Du, H.; Hessler, J. P. *J. Chem. Phys.* **1992**, *96*, 1077.
(63) Ruscic, B.; Wagner, A. F.; Harding, L. B.; Asher, R. L.; Feller, D.; Dixon, D. A.; Peterson, K. A.; Song, Y.; Qian, X.; Ng, C. Y.; Liu, J.; Chen, W.; Schwenke, D. W. *J. Phys. Chem. A* **2002**, *106*, 2727.
(64) Herbon, J. T.; Hanson, R. K.; Golden, D. M.; Bowman, C. T. *Proc. Combust. Inst.* **2002**, *29*, 1201.
(65) Wooldridge, M. S.; Hanson, R. K.; Bowman, C. T. *Int. J. Chem. Kinet.* **1994**, *26*, 389.
(66) Oldenborg, R. C.; Loge, G. W.; Harridine, D. M.; Winn, K. R. *J. Phys. Chem.* **1992**, *96*, 8426.
(67) Michael, J. V.; Su, M.-C.; Sutherland, J. W.; Carroll, J. J.; Wagner, A. F. *J. Phys. Chem. A* **2002**, *106*, 5297.
(68) Srinivasan, N. K.; Su, M.-C.; Sutherland, J. W.; Michael, J. V.; Ruscic, B. *J. Phys. Chem. A* **2006**, *110*, 6602–6607.
(69) Wu, C.-W.; Lee, Y.-P.; Xu, S.; Lin, M. C. *J. Phys. Chem. A* **2007**, *111*, 6693.
(70) Taylor, P. H.; Yamada, T.; Marshall, P. *Int. J. Chem. Kinet.* **2006**, *38*, 489.
(71) Gupte, K. S.; Kiefer, J. H.; Tranter, R. S.; Klippenstein, S. J.; Harding, L. B. *Proc. Combust. Inst.* **2007**, *31*, 167.
(72) Vasudevan, V.; Davidson, D. F.; Hanson, R. K. *Int. J. Chem. Kinet.* **2005**, *37*, 98.
(73) Vasudevan, V.; Davidson, D. F.; Hanson, R. K. *J. Phys. Chem. A* **2005**, *109*, 3352.
(74) Kumaran, S. S.; Carroll, J. J.; Michael, J. V. *Proc. Combust. Inst.* **1998**, *27*, 125.
(75) Krasnoperov, L. N.; Chesnokov, E. N.; Stark, H.; Ravishankara, A. R. *J. Phys. Chem. A* **2004**, *108*, 11526.
(76) Baulch, D. L.; Cobos, C. J.; Cox, R. A.; Esser, C.; Frank, P.; Just, Th.; Kerr, J. A.; Pilling, M. J.; Troe, J.; Walker, R. W.; Warnatz, J. *J. Phys. Chem. Ref. Data* **1992**, *21*, 411.
(77) Srinivasan, N. K.; Su, M.-C.; Sutherland, J. W.; Michael, J. V. *J. Phys. Chem. A* **2005**, *109*, 7902.
(78) Jasper, A. W.; Klippenstein, S. J.; Harding, L. B.; Ruscic, B. *J. Phys. Chem. A* **2007**, *111*, 3932.
(79) Srinivasan, N. K.; Su, M.-C.; Michael, J. V. *Phys. Chem. Chem. Phys.* **2007**, *9*, 4155.
(80) Lim, K. P.; Michael, J. V. *J. Chem. Phys.* **1993**, *98*, 3919.
(81) Fockenberg, C.; Hall, G. E.; Preses, J. M ; Sears, T. J.; Muckerman, J. T. *J. Phys. Chem. A* **1999**, *103*, 5722. (a) Preses, J. M.; Fockenberg, C.; Flynn, G. W. *J. Phys. Chem. A* **2000**, *104*, 6758.
(82) Michael, J. V.; Keil, D. G.; Klemm, R. B. *Int. J. Chem. Kinet.* **1983**, *15*, 705.
(83) Krasnoperov, L. N.; Michael, J. V. *J. Phys. Chem. A* **2004**, *108*, 5643.
(84) Su, M.-C.; Michael, J. V. *Proc. Combust. Inst.* **2002**, *29*, 1219.
(85) Michael, J. V.; Su, M.-C.; Sutherland, J. W.; Harding, L. B.; Wagner, A. F. *Proc. Combust. Inst.* **2005**, *30*, 965.
(86) Sugawara, K.; Okazaki, K.; Sato, S. *Bull. Chem. Soc. Jpn.* **1981**, *54*, 2872.

JP104759D

RATE CONSTANTS FOR THE THERMAL DECOMPOSITION OF ETHANOL AND ITS BIMOLECULAR REACTIONS WITH OH AND D: REFLECTED SHOCK TUBE AND THEORETICAL STUDIES

by

R. Sivaramakrishnan, M.-C. Su,[&] J. V. Michael,[*]

S. J. Klippenstein,[*] L. B. Harding, and B. Ruscic

Supplementary Information

The experimental data are given below in supplementary tables S1-S4.

Table S1: High-T Rate Data: $C_2H_5OH + OH \rightarrow CH_3CHO + H + H_2O$

P_1 / Torr	M_s[a]	ρ_5 / (10^{18} cm^{-3})[b]	T_5 / K[b]	k_{12}[c]	k_{12}[d]	Φ[e]
X_{C2H5OH} = 9.383 x 10^{-5}		$X_{tBH\ Sol`n.}$ = 2.536 x 10^{-5}				
10.89	2.241	1.852	1287	1.620(-11)	1.625(-11)	0.300
10.93	2.251	1.867	1297	1.333(-11)	1.360(-11)	0.310
10.96	2.105	1.728	1150	1.150(-11)	1.100(-11)	0.320
10.92	2.103	1.719	1148	1.103(-11)	1.075(-11)	0.313
10.88	1.970	1.571	1022	1.091(-11)	1.025(-11)	0.310
10.91	2.061	1.674	1108	1.174(-11)	1.070(-11)	0.325
10.86	2.126	1.733	1171	1.244(-11)	1.125(-11)	0.305
10.88	2.059	1.661	1109	1.132(-11)	1.075(-11)	0.310
10.96	1.985	1.599	1036	9.860(-12)	9.850(-12)	0.300
X_{C2H5OH} = 9.383 x 10^{-5}		$X_{tBH\ Sol`n.}$ = 2.536 x 10^{-5}				
15.88	1.999	2.378	1049	1.020(-11)	9.800(-12)	0.318
15.86	1.996	2.370	1045	9.834(-12)	9.800(-12)	0.320
15.97	2.091	2.531	1134	1.056(-11)	1.000(-11)	0.337
15.90	2.126	2.553	1175	1.086(-11)	1.025(-11)	0.335
15.99	2.123	2.562	1172	1.114(-11)	1.030(-11)	0.315
15.92	2.235	2.706	1283	1.118(-11)	1.250(-11)	0.310
15.93	2.183	2.637	1231	1.196(-11)	1.175(-11)	0.300
15.90	2.192	2.644	1240	1.088(-11)	1.075(-11)	0.310
15.92	2.145	2.583	1194	1.180(-11)	1.100(-11)	0.310
15.86	2.105	2.524	1151	1.280(-11)	1.225(-11)	0.308
X_{C2H5OH} = 4.885 x 10^{-5}		$X_{tBH\ Sol`n.}$ = 1.394 x 10^{-5}				
30.98	1.790	3.838	857	9.466(-12)	9.400(-12)	0.325
30.64	1.810	3.889	868	9.843(-12)	9.700(-12)	0.330
30.79	1.849	4.007	907	9.789(-12)	9.650(-12)	0.325
30.67	1.880	4.088	933	9.225(-12)	9.250(-12)	0.320
30.66	1.891	4.120	943	1.080(-11)	1.000(-11)	0.320
30.97	1.901	4.200	951	9.880(-12)	9.850(-12)	0.320

[a]The error in measuring the Mach number, M_s, is typically 0.5-1.0 % at the one standard deviation level. [b]Quantities with the subscript 5 refer to the thermodynamic state of the gas in the reflected shock region. [c]Rate constants: pseudo first order in units cm^3 molecule^{-1} s^{-1}. [d]Rate constants from modeling OH profiles using scheme in Table 4 in units cm^3 molecule^{-1} s^{-1}. [e] $\Phi = X_{tBH} / X_{tBH\ Sol`n}$.

Table S2: High-T Rate Data: D + $C_2H_5OH \rightarrow$ Products

P_1 / Torr	M_s[a]	ρ_5 / (10^{18} cm^{-3})[b]	T_5 / K[b]	k_{13}[c]
X_{C2H5OH} = 8.652 x 10^{-5}		X_{C2D5I} = 5.092 x 10^{-7}		
15.92	2.180	2.615	1236	9.961(-12)
15.92	2.217	2.663	1273	1.162(-11)
15.86	2.300	2.761	1359	1.494(-11)
15.94	2.256	2.719	1314	1.328(-11)
15.88	2.261	2.715	1319	1.370(-11)
15.95	2.174	2.610	1230	9.961(-12)
15.89	2.135	2.545	1192	8.716(-12)
15.88	2.145	2.567	1198	9.131(-12)
15.94	2.105	2.520	1159	8.301(-12)
X_{C2H5OH} = 8.652 x 10^{-5}		X_{C2D5I} = 5.092 x 10^{-7}		
30.78	2.188	4.977	1222	9.546(-12)
30.92	2.154	4.908	1188	7.969(-12)
30.83	2.087	4.710	1124	7.471(-12)
30.83	2.023	4.528	1064	5.728(-12)
30.82	2.052	4.595	1095	7.139(-12)
X_{C2H5OH} = 8.349 x 10^{-5}		X_{C2D5I} = 4.997 x 10^{-7}		
30.90	2.012	4.506	1054	6.641(-12)
30.75	2.123	4.797	1158	8.301(-12)
30.70	2.100	4.726	1136	7.886(-12)

[a]The error in measuring the Mach number, M_s, is typically 0.5-1.0 % at the one standard deviation level. [b]Quantities with the subscript 5 refer to the thermodynamic state of the gas in the reflected shock region. [c]Rate constants from modeling D profiles using scheme in Table 4 in units cm^3 $molecule^{-1}$ s^{-1}.

Table S3: High-T Rate Data: $C_2H_5OH + M \rightarrow C_2H_4 + H + OH + M$

P_1 / Torr	M_s[a]	ρ_5 / (10^{18} cm^{-3})[b]	T_5 / K[b]	k_3[c]
X_{C2H5OH} = 1.155 x 10^{-4}				
10.95	2.340	1.954	1392	5.117(-18)
X_{C2H5OH} = 2.257 x 10^{-4}				
10.89	2.479	2.051	1555	4.875(-17)
X_{C2H5OH} = 3.736x 10^{-4}				
10.89	2.442	2.037	1502	3.683(-17)
10.92	2.582	2.157	1663	1.855(-16)
10.88	2.459	2.049	1521	3.904(-17)
X_{C2H5OH} = 2.341 x 10^{-4}				
15.94	2.391	2.909	1445	1.031(-17)
15.83	2.470	2.981	1530	3.355(-17)
15.88	2.461	2.981	1521	3.355(-17)
15.91	2.402	2.917	1456	1.714(-17)

[a]The error in measuring the Mach number, M_s, is typically 0.5-1.0 % at the one standard deviation level. [b]Quantities with the subscript 5 refer to the thermodynamic state of the gas in the reflected shock region. [c]Rate constants: bimolecular in units cm^{3}molecule^{-1} s^{-1}.

Table S4: High-T Rate Data: $C_2H_5OH \rightarrow C_2H_4 + H_2O$, $C_2H_5OH \rightarrow CH_3 + CH_2O + H$

P_1 / Torr	M_s[a]	ρ_5 / (10^{18} cm^{-3})[b]	T_5 / K[b]	k_1[c]	k_2[c]	$BR_{2,3}$[d]
X_{C2H5OH} = 2.339 x 10^{-6}						
5.94	2.636	1.192	1732	10500	4184	0.300
5.93	2.522	1.142	1597	6750	2178	0.250
5.94	2.507	1.137	1579	4290	1153	0.220
5.92	2.394	1.082	1451	1691	400	0.195
5.94	2.333	1.060	1381	840	157	0.160
5.71	2.403	1.051	1457	3075	665	0.180
5.97	2.418	1.106	1473	2460	527	0.180
X_{C2H5OH} = 1.025 x 10^{-6}						
10.96	2.306	1.917	1361	424	121	0.230
10.87	2.500	2.076	1571	5040	1822	0.280
10.87	2.471	2.052	1538	5181	1331	0.215
10.93	2.483	2.073	1551	3876	1119	0.240
10.98	2.377	1.991	1433	1615	267	0.150
10.89	2.387	1.984	1444	1200	279	0.200
10.90	2.478	2.070	1540	3420	989	0.240
10.89	2.391	1.987	1448	2187	490	0.190
10.94	2.435	2.034	1497	2340	611	0.220
10.94	2.352	1.962	1406	1290	199	0.140
10.90	2.475	2.061	1542	6105	2052	0.260
10.94	2.594	2.164	1681	12420	5068	0.310
X_{C2H5OH} = 2.339 x 10^{-6}						
10.89	2.339	1.947	1386	731	111	0.140
10.9	2.549	2.128	1623	7097	2039	0.245
10.94	2.395	2.000	1452	2053	473	0.195
10.77	2.521	2.074	1596	6503	1808	0.235
10.84	2.458	2.035	1523	3100	829	0.225
10.87	2.371	1.970	1421	1260	226	0.160
10.91	2.367	1.980	1417	850	137	0.150
X_{C2H5OH} = 1.025x 10^{-6}						
15.89	2.420	2.930	1479	1884	455	0.215
15.90	2.414	2.935	1467	1774	326	0.175
15.78	2.328	2.809	1375	1104	86	0.08
15.91	2.348	2.856	1396	792	93	0.12
15.87	2.387	2.897	1438	1408	160	0.12
15.90	2.401	2.919	1453	1868	342	0.17
15.89	2.502	3.033	1563	3850	943	0.23
15.97	2.557	3.109	1626	8195	2343	0.255
X_{C2H5OH} = 6.470x 10^{-7}						
15.89	2.503	3.034	1564	4575	1315	0.250

15.90	2.519	3.054	1583	5325	1906	0.290
15.94	2.541	3.586	1607	8750	3384	0.300
$X_{C2H5OH.}$ = 2.339 x 10^{-6}						
15.99	2.263	2.763	1308	107	11	0.110
15.99	2.368	2.900	1418	1050	128	0.125
15.84	2.371	2.870	1421	860	116	0.140
$X_{C2H5OH.}$ = 6.470 x 10^{-7}						
30.86	2.450	5.663	1486	3488	884	0.225
30.8	2.368	5.463	1398	1485	286	0.175
30.97	2.374	5.507	1404	1733	485	0.230
30.84	2.554	5.885	1601	6900	2450	0.310
30.8	2.387	5.507	1418	1501	358	0.210
30.86	2.291	5.286	1318	595	49	0.085

[a]The error in measuring the Mach number, M_s, is typically 0.5-1.0 % at the one standard deviation level. [b]Quantities with the subscript 5 refer to the thermodynamic state of the gas in the reflected shock region. [c]Rate constants: First order in s^{-1}. [d] $BR_{2,3} = k_2+k_3 / (k_1+k_2+k_3)$.